Environmental Data Science (2026), 5: e7, 1–25
doi:10.1017/eds.2026.10034

CAMBRIDGE UNIVERSITY PRESS

APPLICATION PAPER

Combined effects of site and model parameterization for soil respiration components in a Canadian wildfire chronosequence

John Zobitz[1], Xuan Zhou[2], Heidi Aaltonen[3], Egle Köster[4], Frank Berninger[2], Jukka Pumpanen[5] and Kajar Köster[2]

[1]Department of Mathematics, Computer Science, and Data Science, Augsburg University, Minneapolis, USA
[2]Department of Environmental and Biological Sciences, University of Eastern Finland, Joensuu, Finland
[3]Department of Agricultural Sciences, University of Helsinki, Helsinki, Finland
[4]School of Forest Sciences, University of Eastern Finland, Joensuu, Finland
[5]Department of Environmental and Biological Sciences, University of Eastern Finland, Kuopio, Finland
Corresponding author: Kajar Köster; Email: kajar.koster@uef.fi

Received: 15 August 2024; **Revised:** 13 February 2026; **Accepted:** 01 March 2026

Keywords: carbon; data assimilation; microbes; modeling; soil respiration

Abstract

Forest fires alter soil organic carbon and suppress soil respiration for decades following disturbance. However, uncertainties in model parameterization and sensitivity hinder robust predictions of autotrophic and heterotrophic soil respiration responses. We addressed this challenge using a novel dataset from a fire chronosequence in the Yukon and Northwest Territories of Canada. The dataset included field measurements of total soil respiration at four sites with varying time since fire, supplemented by field measurements of soil temperature at two depths, remote sensing data on aboveground productivity, and soil moisture at two depths. We evaluated a suite of soil respiration models, ranging from exponential Q_{10} formulations to heterotrophic respiration models using Michaelis–Menten kinetics. To estimate parameters efficiently, we (1) derived algebraic expressions for soil respiration components assuming quasi-steady state dynamics and (2) applied a Markov Chain Monte Carlo (MCMC) approach for parameter estimation. The resulting parameter estimates revealed which parameters were well-constrained and where uncertainty remained. Modeled respiration agreed with established empirical relationships and highlighted two key findings: (1) all chronosequence sites favored models that explicitly included microbial carbon as a distinct pool, and (2) parameters related to aboveground litter inputs were better constrained than those for root turnover. These results held regardless of soil depth or the form of the autotrophic respiration moisture response. These findings indicate that direct field measurements of litterfall rates would reduce model uncertainty, and that targeted sampling during seasonal transitions (e.g., freeze–thaw periods) would provide critical constraints on microbial activity when respiration dynamics are most variable.

Impact Statements

When developing mathematical models of ecological systems, a common guiding principle is starting with a simple first model and then adding complexity to the model. We apply that principle here with models of permafrost soil carbon at four remote northern hemisphere sites. These sites are interesting ecologically because

This Application Paper was awarded Open Data and Open Materials badges for transparent practices. See the Data Availability Statement for details.

© The Author(s), 2026. Published by Cambridge University Press. This is an Open Access article, distributed under the terms of the Creative Commons Attribution licence (http://creativecommons.org/licenses/by/4.0), which permits unrestricted re-use, distribution and reproduction, provided the original article is properly cited.

https://doi.org/10.1017/eds.2026.10034 Published online by Cambridge University Press

northern hemisphere permafrost soils have comparatively more carbon than soil from other regions and remain frozen for much of the year. Forest fires in these areas affect soil carbon levels by changing how deep the soil freezes and also adding burned organic material to the soil. Vegetation regrowth increases soil carbon in the years following the initial fire disturbance, leading to measurable changes in soil respiration. Our study design included four forest sites at different times since the last recorded forest fire. Previous measurements of soil respiration showed differences in the amount of total soil respiration at these sites. Here, we apply a series of mathematical models with a parameter estimation method to quantify annual patterns in the contribution of soil respiration from roots or microbes. Our results showed a preference for more complex models of soil carbon that apply empirical or process-based relationships between litter inputs, soil microbes, and soil heterotrophic respiration.

1. Introduction

At present, net exchanges among the terrestrial, oceanic, and atmospheric carbon pools partially offset anthropogenic carbon emissions, thereby moderating the growth of atmospheric carbon dioxide concentrations (Friedlingstein et al., 2025). Although uncertainties remain across all components of the global carbon cycle, long-term ecological observation networks (e.g., FLUXNET, the Integrated Carbon Observation System, and the National Ecological Observatory Network) are essential for reducing these uncertainties and providing critical constraints for Earth system model predictions. However, reconciling differences among model-derived and data-driven estimates of terrestrial carbon fluxes remains a major scientific priority (Jian et al., 2022a).

One component of the terrestrial carbon cycle is soil heterotrophic (microbial) respiration from organic matter decomposition, denoted as R_H. Total soil respiration, R_S, represents the contributions of several components: soil autotrophic respiration (R_A), microbial growth respiration (R_G), and heterotrophic respiration (R_H); thus $R_S = R_A + R_H + R_G$. Earth system models estimate global soil heterotrophic respiration (R_H), often producing a range of values that align broadly with empirical estimates of total soil respiration (R_S) (Shao et al., 2013), despite differing model assumptions and parameterizations. This convergence in modeled R_H, despite structural and parametric differences among models, it exemplifies model equifinality (Beven and Freer, 2001; Tang and Zhuang, 2008; Luo et al., 2009; Marschmann et al., 2019; Famiglietti et al., 2021). While such broad agreement among models is encouraging, it also poses a challenge for determining which process representations for R_H are most appropriate in a given context.

Model equifinality in soil respiration projections arises from the diverse ways in which components of R_S are represented in models. These differences are key contributors to forecast uncertainty (Shi et al., 2018; Sulman et al., 2018). Many models apply an exponential Q_{10} functional relationship to describe the temperature sensitivity of soil respiration (Davidson et al., 2006). Often the Q_{10} value is assumed to be static across the soil biome (Bond-Lamberty et al., 2004a; Chen and Tian, 2005; Hamdi et al., 2013). Other models (in conjunction with or as alternatives to a Q_{10} model) include linear regression of R_S with other measured covariates (van Wijk et al., 2008; Köster et al., 2017); highly structured models of interacting soil microbes (Allison, 2012); genomic-based metabolic models (Zomorrodi and Segrè, 2016); or coupling soil microbial communities to aboveground biogeochemical processes and structured soil carbon pools (Fang and Moncrieff, 2001; Bosatta and Ågren, 2002; Zobitz et al., 2008; Allison, 2012; Todd-Brown et al., 2012; Wutzler and Reichstein, 2013; Sihi et al., 2016; Zobitz et al., 2021).

Representations of R_S and its component fluxes inevitably involve simplifying assumptions regarding biological and physical processes. As a result, the range of modeling approaches mirrors both the pronounced spatial heterogeneity of soils and the persistent difficulty of defining formulations that apply broadly across ecosystems. To address and reduce model equifinality, previous studies have applied the same model across a range of sites (Shao et al., 2013; Sihi et al., 2016; Jian et al., 2020), conducted model intercomparison studies (Friedlingstein et al., 2006; Trudinger et al., 2007; Schwalm et al., 2010), or developed a unified modeling framework to facilitate systematic intercomparisons across models (Todd-Brown et al., 2012). Taken together, these approaches provide a basis for evaluating how differences in site conditions and model structure contribute to variation in model outputs.

https://doi.org/10.1017/eds.2026.10034 Published online by Cambridge University Press

This study evaluates model equifinality in soil respiration models using a set of focal sites in northern high-latitude forests. Permafrost soils in these regions store approximately 1600 Pg of carbon—about 35% of the global soil carbon pool (Schuur et al., 2008; Fan et al., 2020)—despite occupying only ~22% of the Northern Hemisphere land area (Obu et al., 2019). This disproportionate carbon storage underscores the outsized influence of high-latitude ecosystems on the terrestrial carbon cycle. Improving model representations of soil respiration in these regions is therefore critical for reducing uncertainties in global carbon cycle projections and for addressing knowledge gaps in global soil carbon fluxes (Bond-Lamberty, 2018; Warner et al., 2019).

Respiration of permafrost soils is strongly influenced by the successional stage following fire disturbance. Immediately after a fire, the release of pyrogenic carbon alters soil organic matter quality, which in turn reduces heterotrophic respiration in permafrost soils (Holden et al., 2016; Song et al., 2019; Zhao et al., 2021). After decades of vegetation regrowth, microbial carbon ultimately stabilizes (Ribeiro-Kumara et al., 2020). Additionally, fire disturbance and subsequent vegetation regrowth modify environmental drivers (e.g., soil organic carbon, soil temperature, and soil moisture) of respiration (Aaltonen et al., 2019a, 2019b). Thawed permafrost soil also provides substrate for increased soil autotrophic and heterotrophic (microbial) respiration (Schaefer and Jafarov, 2016; Walker et al., 2019). Temporal patterns in R_A and R_H are also influenced by soil heterogeneity in these high-latitude soils (e.g., permafrost versus non-permafrost soils, bacterial versus fungal species composition).

This study examines the combined effects of site-specific variability (indicated by time since fire disturbance) and model parameterization of soil respiration in permafrost soils. We use a chronosequence dataset collected at a high-latitude forest in Canada (Köster et al., 2017; Aaltonen et al., 2019a, 2019b). The dataset includes field measured soil respiration measurements. We index field sites by when a stand-replacing fire last occurred.

Zobitz et al. (2021) previously parameterized three static soil respiration submodels (collectively called FireResp), each reflecting varying assumptions about soil structure (e.g., a single soil carbon pool, multiple soil carbon pools, or a distinct microbial carbon pool). That study emphasized evaluating model parameters against observed field soil respiration and soil carbon observations. Unlike FireResp, for this study, we are investigating changes in respiration over time, which will require additional considerations in how respiration is calculated. To that end, we developed a new model (called FireGrow) that models soil respiration components over multiple years with site-specific environmental forcing variables. The FireGrow model applies foundational assumptions of quasi-steady state analysis to develop algebraic expressions for soil respiration that are not functionally dependent on soil carbon stock size (which could not be measured continuously at our site). Here we use the same chronosequence dataset as Zobitz et al. (2021), supplemented with daily soil temperature observations (Köster et al., 2017) at two depths (5 and 10 cm). These temperature data, combined with remote sensing observations, enable us to construct a multi-year timeseries of environmental forcing variables to parameterize components of soil respiration.

With these additional data, we analyze annual patterns of modeled soil respiration and its components after applying a parameter estimation method. We parameterize the models at each site using either previously established parameter values (Zobitz et al., 2021) or through Markov Chain Monte Carlo (MCMC) parameter estimation. This approach balances factorial complexity (four sites, three models, and two depths) with computational complexity.

To examine the combined effects of site variability and model structure on parameterization, we address two key questions. First, how does site-specific variability across a fire chronosequence influence the parameterization of a soil carbon model? We explore this by analyzing the accepted parameter distributions for each model across the chronosequence. Second, how does model structure influence the predicted components of soil respiration? To answer this, we evaluate model outputs across the chronosequence and compare them to empirically expected relationships. This study advances understanding of methods for modeling permafrost soil respiration in relation to forest successional age following stand-replacing fires. Considering the challenges of remote site access, we present frameworks that optimize the information content derived from the available data, providing a roadmap for future validation studies. These approaches broadly support the identification of the "best approximating model"

https://doi.org/10.1017/eds.2026.10034 Published online by Cambridge University Press

(Burnham and Anderson, 2002) for soil organic matter decomposition, particularly when utilizing diverse models and datasets.

2. Methods

2.1. Study sites

We collected data from a transect of sites in the northern boreal forests of Canada (Figure 1), located near Eagle Plains, Yukon (66° 220′ N, 136° 430′ W), and Tsiigehtchic, Northwest Territories (67° 260′ N, 133° 450′ W). This transect was established in 2015 (Köster et al., 2017). The study sites were chosen based on maps from the Canadian Wildfire Information System (Natural Resources Canada, 2021), selected for site accessibility and time since the last fire. The mean annual air temperature at these sites is −8.8 °C. The sites are evergreen coniferous forests dominated by *Picea mariana* (Mill.) BSP and *Picea glauca* (Moench) Voss species. Chronosequence sites were selected from the time since last burned with a stand replacing fire (in 1968, 1990, and 2012) and included a control site, where the last fire was more than 100 years ago. For this manuscript, and similar to Aaltonen et al. (2019b), Köster et al. (2017), and Zobitz et al. (2021), a chronosequence site will be identified by the year it was burned (2012, 1990, 1968) or the control site as "Control." Our analysis will compare differences between modeling results at each chronosequence site.

In the summer of 2015 we established three different lines at each chronosequence site, and within each line, three replicate plots (Köster et al., 2017). At each plot we installed metal collars; the lower edge of the collar was placed 0.02 m depth in the mor layer above the rooting zone to avoid damaging the roots (Köster et al., 2017). Soil CO_2 fluxes (R_S) were measured with static cylindrical chambers. As described in Köster et al. (2017), a cylindrical chamber was inserted above each collar. When measuring we did not remove or damage vegetation inside the chamber. We then sampled chamber CO_2 concentrations with a non-dispersive infrared CO_2 probe (GMP343, Vaisala Oyj, Helsinki, Finland) at 5 second intervals for 4 minutes during the 5 minute chamber deployment time. For subsequent reporting the first 30 seconds after placing the chamber onto the collar were discarded to exclude disturbance effects of chamber deployment. For model parameterization, we calculated the median R_S across the three replicate plots at each measurement line within a chronosequence site. Median R_S values from different measurement lines within a site were assumed to be independent.

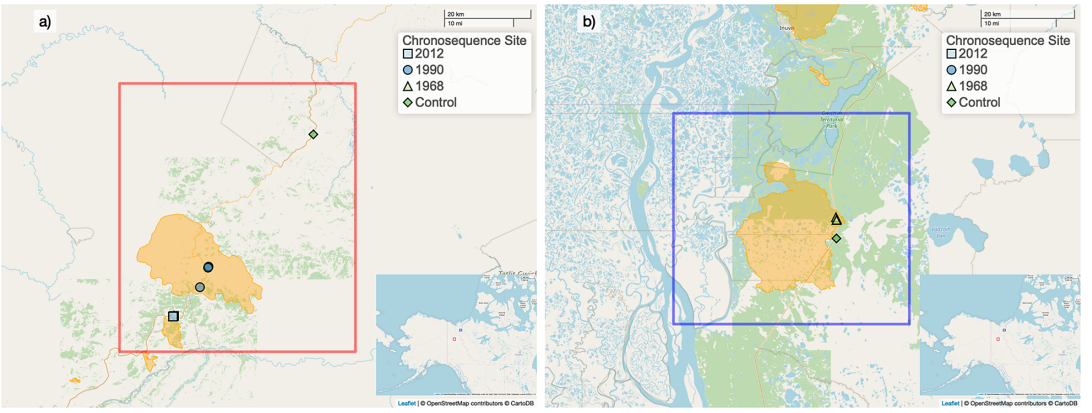


Figure 1. *Map of chronosequence site locations in the Yukon and the Northwest Territories of Canada. For both maps, orange areas demarcate the areal extent of the forest fire. Panel a) illustrates the southern chronosequence sites that were burned in 1968 (triangles), 1990 (circles), 2012 (squares), and a Control site (diamonds). Panel b) illustrates the northern sites, which contains chronosequence sites that were burned in 1968 (triangles) and an additional Control site (diamonds). Maps provided by © OpenStreetMap contributors © CartoDB.*

https://doi.org/10.1017/eds.2026.10034 Published online by Cambridge University Press

In addition, we measured soil temperature (5 and 10 cm depth) in four hour intervals at three chronosequence sites (Control, 2012, 1990) with iButton (model DS1921G-F5, precision: 0.5 ° C, accuracy: ± 1.0 ° C) temperature sensors (Maxim Integrated, San Jose, California, USA). Temperature sensors were waterproofed with a clear plastic tool dip (Plasti Dip, Plasti Dip International, Blaine, MN, USA) before installing them into the soil (Köster et al., 2024). The observed soil temperature data were used to parameterize soil diffusivity, and in turn, an annual pattern of soil temperature at each chronosequence site (see Supplementary Information). Together with the chronosequence site (2012, 1990, 1968, or Control), soil temperature measurement depth (5 or 10 cm) is another categorical variable in our analysis.

2.2. Forcing datasets

At each chronosequence site we derived an annual pattern of key environmental forcing variables: 5 and 10 cm soil temperature (T_S; °C), gross primary productivity (F_{GPP}; g C m^{-2} d^{-1}), and soil water content (*SWC*; %). Soil temperature was directly measured at chronosequence sites; measured data were used to reproduce daily values following an annual cycle as described in the Supplementary Information. The variables F_{GPP} and *SWC* are completely derived from the MODIS products as described directly below.

2.2.1. MODIS and derived data products

We accessed remote sensing products from the AppEEARS web service (AppEEARS Team, 2022) by selecting from MODIS pixels located at each of the different sites in the chronosequence. For model analysis and evaluation, remote sensing products were accessed over the timeperiod January 1, 2015 to December 31, 2021. MODIS products are reported on an 8-day interval. At a chronosequence site, we grouped separate measurement lines (Section 2.1) together, thereby pooling the data approach. Three different types of remote sensing products were accessed: gross primary productivity (F_{GPP}), land surface temperature (*LST*), and the Normalized Difference Vegetation Index (*NDVI*). Of these three, F_{GPP} was a primary input to the FireGrow model and the other two were used to approximate *SWC*.

- Gross Primary Productivity (F_{GPP}): we accessed 500 meter MODIS Terra (MOD17A2H Collection 6, (Running et al., 2022a) and MODIS Aqua MYD17A2H Collection 6, (Running et al., 2022b) gross primary productivity. A *GPP* observation is calculated from derived measurements of photosynthetic fraction of absorbed radiation, taking into account the temperature and vapor pressure deficit from NASA's Global Modeling and Assimilation Office (Running and Zhao, 2019). Here, MODIS *GPP* is divided by eight to report units as g C m^{-2} d^{-1}. For quality assurance, we selected F_{GPP} observations based on the "very best" or "good" quality control bit; we excluded observations when mixed clouds were present or the cloud state could not be determined. Additionally the value of F_{GPP} was set to 0 when the land surface temperature was below 0 °C.
- Land Surface Temperature (*LST*): we accessed 500 meter MODIS Terra (MOD11A2, Wan et al. [2015a]) and MODIS Aqua (MYD11A2, Wan et al. [2015b]) land surface temperature. Values of *LST* are derived from surface emissivity from MODIS bands 31 and 32 with corrections based on atmospheric and emissivity effects for different land cover types (Wan, 1999). For quality assurance, we selected *LST* observations when the average emissivity error was less than 0.04 and the average *LST* error was less than 2 Kelvin (Wan, 2013).
- Normalized Difference Vegetation Index (NDVI): we accessed 500 meter MODIS Terra (MOD09GA, Vermote and Wolfe [2022a]) and MODIS Aqua (MYD09GA, Vermote and Wolfe [2022b]) surface reflectance for the first two MODIS reflectance bands (ρ_1 and ρ_2). The reflectance data products were filtered using the MODLAND "good" quality assurance flags for both the data quality and all eight state flags. The NDVI value was calculated by $NDVI = \frac{\rho_2 - \rho_1}{\rho_2 + \rho_1}$.

MODIS pixels measure 500 meters by 500 meters and may encompass a mix of unburned and burned vegetation. At each chronosequence site (orange areas in Figure 1, we visually verified that MODIS pixels were contained within fire boundaries reported by the Canadian Wildfire Information System (Natural

https://doi.org/10.1017/eds.2026.10034 Published online by Cambridge University Press

Resources Canada, 2021). For the Control, 1968, and 1990 chronosequence sites, the MODIS pixels were located entirely within the reported fire boundaries. However, at the 2012 chronosequence site, visual verification revealed that the MODIS pixel corresponding to the sampling location included a substantial area outside the fire boundary. Consequently, at the 2012 site, we compared F_{GPP} from this MODIS pixel to a pixel located entirely within the fire area. Timeseries analyses of F_{GPP} during 2012 (the reported fire year) showed no decline in F_{GPP} for MODIS pixels outside the fire boundary (see Supplementary Information). Therefore, we refined our analysis by selecting MODIS pixels fully contained within the 2012 fire's areal extent.

MODIS observations of *LST*, *GPP*, and *NDVI* are reported on an 8-day timestep; we applied a smoother to produce daily observations using a modified Tikhonov regularization problem (Tikhonov, 1977; Zobitz et al., 2019), as detailed in the Supporting Information.

The *LST* and *NDVI* products are used to determine the temperature vegetation dryness index (*TVDI*) (Sandholt et al., 2002; Zhang et al., 2014), which we assume is a proxy for the driver variable soil water content (*SWC*). Computation of the *TVDI* is completed by binned regressions between *NDVI* and *LST*. See the Supporting Information for more information on the computation of *SWC*.

2.3. FireGrow model

The FireGrow model is a process-based daily soil carbon model, evaluated from 1 January 2015 to 31 December 2021. We selected 2015 as the starting year that field measurements were taken (Section 2.1). FireGrow model inputs include gross primary productivity F_{GPP}, soil temperature T_S (measured at the 5 or 10 cm depth), and soil water content *SWC*; these inputs vary each day (Section 2.2). Figure 2 shows a timeseries of all dynamic forcing variables for the model evaluation period (1 January

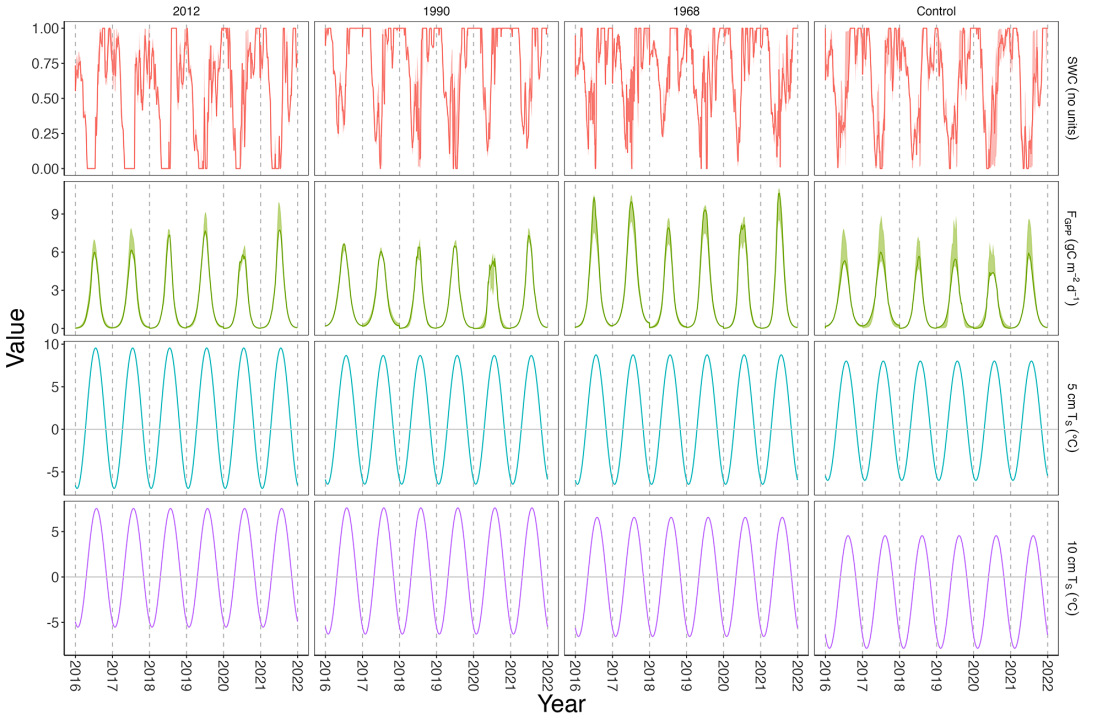


Figure 2. *Timeseries of input variables (SWC, F_{GPP}, or T_S at 5 or 10 cm depth) for the FireGrow model across the model evaluation period (1 January 2016–31 December 2022). Observations of F_{GPP} and SWC include the 95% confidence interval for F_{GPP} and SWC, which represents the 95% confidence interval over all MODIS pixels for that particular site.*

https://doi.org/10.1017/eds.2026.10034 Published online by Cambridge University Press

2015–31 December 2021). For this study, litter rates (i.e., litter from vascular plants, moss and lichens, or living trees) are assumed to be constant and are estimated using the parameter optimization method described in Section 2.4.

FireGrow consists of three different submodels of soil carbon cycling (termed Null, Microbe, and Quality), conceptually shown in Figure 3. These submodels share the same compartmental structure as

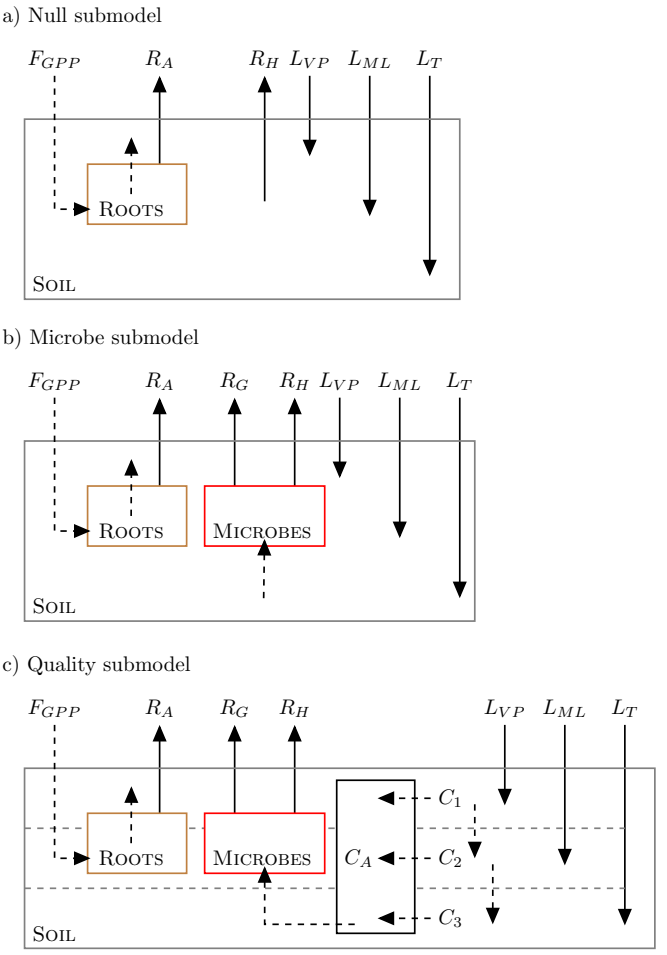


Figure 3. *Conceptual diagrams of the different submodels examined in the FireGrow model. Boxes represent the different soil carbon pools in each submodel. For all models, input rates include gross primary productivity (F_{GPP}), vascular plant litter (L_{VP}), moss and lichen litter (L_{ML}), and living tree litter (L_T). Output rates include autotrophic respiration (R_A), microbe growth respiration (R_G), and microbe heterotrophic respiration (R_H). All rates are represented with solid arrows. Dashed arrows represent transformation processes to each pool (see Supplementary Information for a detailed description of the model). The Null submodel (panel a) considers two soil carbon pools (roots and soil). The Microbe submodel (panel b) includes a separate bulk carbon pool for soil carbon microbes (Microbes box in red). Finally the Quality submodel (panel c) differentiates the soil into four additional soil carbon pools (C_1, C_2, C_3, and C_A). Pools C_1, C_2, and C_3 represent soil carbon with increasing recalcitrance. Soil transformation from C_1, C_2, or C_3 are inputs to C_A, which is a buffer pool of carbon accessible to microbes. In the process of decomposition, a portion of C_1 and C_2 transitions into C_2 and C_3, respectively. Litter input rates (L_{VP}, L_{ML}, and L_T) are assigned to C_1, C_2, or C_3 based on their assumed decomposition rate.*

https://doi.org/10.1017/eds.2026.10034 Published online by Cambridge University Press

those presented in Zobitz et al. (2021), but differ in two important ways. First, in this study, we began with a dynamic formulation to capture temporal changes in carbon pools. Second, we applied a quasi-steady state approximation to express soil respiration components (autotrophic, microbial heterotrophic, or microbial growth respiration) as a function of parameters and our forcing datasets (independent of soil carbon pool size). The quasi-steady state approach applied here matched our available observational constraints. See Section 5 of the Supplementary Information for an additional detailed description of each submodel and how the quasi-steady state approximation is applied.

Submodels differ in two main ways: (1) the inclusion of a structured soil carbon pool with a distinct microbial component, and (2) the treatment of soil carbon substrate, which varies according to litter inputs from different organic sources such as vascular plants, mosses, and lichens, or trees. Model outputs include autotrophic respiration (R_A), microbe heterotrophic respiration (R_H), microbe growth respiration (R_G), and total soil respiration ($R_S = R_A + R_G + R_H$). We assume $R_A = 0$ in frozen soils.

Table 1 in Section 2.4 lists all model parameters in the FireGrow model and associated submodel (Null, Microbe, Quality). Additionally, Section 5 in the Supplementary Information outlines all intermediate steps to derive expressions for R_A, R_H, and R_G for each submodel.

Autotrophic respiration (R_A, gC m^{-2} d^{-1}) is defined with Equation 2.1:

$$R_A = \frac{g_R}{g_R + \delta_R}(\alpha - \beta)F_{GPP}, \tag{2.1}$$

where the parameter α represents root growth and the parameter β is root exudation. As described in the Supplementary Information, here we set $\alpha = 0.2$ and $\beta = 0.1$. The parameter δ_R represents root turnover (yr^{-1}; converted to d^{-1} for subsequent calculations). For convenience in representation, the term g_R is a combination of model parameters (Equation 2.2):

$$g_R = k_R \cdot Q_{10,R}^{(T_S - 10)/10} \cdot h(SWC) \tag{2.2}$$

Equation 2.2 defines k_R as the parameter representing the root (autotrophic) kinetic rate constant (d^{-1}) and $Q_{10,R}$ as the parameter representing the dimensionless Q_{10} value. Additionally, Equation 2.2 also modifies respiration according to soil water content (SWC, %) with the empirical equation $h(SWC) = 3.11SWC - 2.42SWC^2$ (Moyano et al., 2013). The equation $h(SWC)$ was the same at all chronosequence sites and soil depths (5 or 10 cm). To evaluate whether the empirical relationship $h(SWC) = 3.11, SWC - 2.42, SWC^2$ introduces bias in modeled annual soil flux patterns, we tested alternative formulations of $h(SWC)$ in Section 8 of the Supplementary Information, setting $h(SWC) = SWC$ or $h(SWC) = 1$. Results from these alternatives are discussed further in Section 3.

The Null submodel (Figure 3a) makes no distinction between microbial or soil carbon (Davidson et al., 1998; Reichstein and Beer, 2008), and as a result no distinction between R_H and R_G. Heterotrophic respiration R_H is described by Equation 2.3:

$$R_H = \beta F_{GPP} + L_{VP} + L_{ML} + L_T + \frac{\delta_R}{g_R + \delta_R}(\alpha - \beta)F_{GPP} \tag{2.3}$$

In Equation 2.3, L_{VP} is vascular plant litter, L_{ML} moss and lichen litter, and L_T living tree litter (all have units gC m^{-2} d^{-1}). Together with R_A (Equation 2.1), the Null model is represented with Equation 2.4:

$$\begin{aligned} R_A &= \frac{g_R}{g_R + \delta_R}(\alpha - \beta)F_{GPP} \\ R_H &= \beta F_{GPP} + L_{VP} + L_{ML} + L_T + \frac{\delta_R}{g_R + \delta_R}(\alpha - \beta)F_{GPP} \\ R_S &= R_A + R_H \end{aligned} \tag{2.4}$$

The Microbe submodel (Figure 3b) differentiates soil carbon into root carbonsoil carbon (C_S), and microbial carbon (C_M, gC m^{-2} d^{-1}). Microbes transform soil carbon into biomass through Michaelis–Menten kinetics (Michaelis and Menten, 1913; Davidson et al., 2006; German et al., 2012). A proportion ϵ (unitless) of this transformed amount is directly respired as growth respiration (R_G), and the remaining

https://doi.org/10.1017/eds.2026.10034 Published online by Cambridge University Press

https://doi.org/10.1017/eds.2026.10034 Published online by Cambridge University Press

Table 1. *Description of parameters used for the FireGrow model*

Name	Description (units)	2012	1990	1968	Control	Notes
Estimated from literature						
α	Allocation parameter (proportion of GPP) (no units)	0.2	0.2	0.2	0.2	(Zhang et al., 2009; Zobitz et al., 2021)
β	Exudation parameter (proportion of GPP) (no units)	0.1	0.1	0.1	0.1	(Zhang et al., 2009; Zobitz et al., 2021)
k_1	transfer rate from C_1 to C_A (yr^{-1})	0.1718	0.1718	0.1718	0.1718	(Elzein and Balesdent, 1995)
k_2	transfer rate from C_2 to C_A (yr^{-1})	0.00732	0.00732	0.00732	0.00732	(Elzein and Balesdent, 1995)
k_3	transfer rate from C_3 to C_A (yr^{-1})	0.00001	0.00001	0.00001	0.00001	(Elzein and Balesdent, 1995)
Estimated in (Zobitz et al., 2021)						
$Q_{10,R}$	Root Q_{10} (no units)	(1.3,3.7,1.3)	(1,5,1)	(2.1,1.5,1.5)	(1,1,1)	5 cm soil depth
		(2.6,1.1,2.2)	(1,5,5)	(3.7,4.2,4.0)	(1,1,1)	10 cm soil depth
Estimated in this study			Allowed range			
L_{VP}	Vascular plants litter rate (d^{-1})		$0-0.6$			
L_{ML}	Moss and lichen litter rate (d^{-1})		$0-0.6$			
L_T	Living trees litter rate (d^{-1})		$0-0.6$			
δ_R	Root turnover rate (yr^{-1})		$0-0.5$			
k_R	Kinetic root (autotropic) rate constant (d^{-1})		$0-0.1$			
ϵ	microbial efficiency (no units)		$0-1$			
r_1	transfer rate from C_1 to C_2 (d^{-1})		$0-0.1$			
r_2	transfer rate from C_2 to C_3 (d^{-1})		$0-0.2$			

Note. For parameters estimated in Zobitz et al. (2021), parameter values for each chronosequence site (2012, 1990, 1968, Control) are reported as an ordered triplet according to the Null, Microbe, and Quality submodels, respectively. The allowed range at each site was the same for each model when parameters were estimated with the modified Metropolis-Hastings methods.

$1-\epsilon$ incorporated into microbe biomass C_M. From the quasi-steady state assumptions, Equation 2.5 shows together heterotrophic respiration (R_H), microbial growth respiration (R_G), and autotrophic respiration (R_A; Equation 2.1):

$$\begin{aligned} R_A &= \frac{g_R}{g_R+\delta_R}(\alpha-\beta)F_{GPP} \\ R_H &= (1-\epsilon)\left(\beta F_{GPP} + L_{VP} + L_{ML} + L_T + \frac{\delta_R}{g_R+\delta_R}(\alpha-\beta)F_{GPP}\right) \\ R_G &= \epsilon\left(\beta F_{GPP} + L_{VP} + L_{ML} + L_T + \frac{\delta_R}{g_R+\delta_R}(\alpha-\beta)F_{GPP}\right) \\ R_S &= R_A + R_H + R_G \end{aligned} \tag{2.5}$$

The Quality submodel (Figure 3c) parameterizes the soil carbon into different pools based on the recalcitrance and turnover time of the soil parent material, similar to models by Bosatta and Ågren (1985). The Quality submodel has four broad pools of carbon (C_1, C_2, C_3, and C_A, all units gC m^{-2} d^{-1}), ranging from labile carbon (C_1) to recalcitrant (C_3). We associate C_1 with soil carbon with a short turnover time (that is dissolved organic carbon or fresh plant residues) and C_3 with a longer turnover time, such as humic substances and biochar (McLauchlan and Hobbie, 2004; Ferraz de Almeida et al., 2019; Wang et al., 2019). The pool C_A is a buffer pool of carbon accessible to microbes. Similar to the Microbe submodel, microbes transform soil carbon from C_A into biomass through Michaelis–Menten kinetics. Transformation of soil carbon pools C_1, C_2, C_3 occurs through turnover to C_A (at a rate k_1C_1, k_2C_2, or k_3C_3 with k_1, k_2, or k_3 all having units yr^{-1} respectively; converted to d^{-1} for subsequent calculations) and mineralization from pool C_X to pool C_{X+1} (by r_XC_X, r_X units day^{-1}), where X equals 1 or 2. Based on a mechanistic model in Elzein and Balesdent (1995), we set k_1, k_2, and k_3 as an average of reported turnover rates across a three-compartment soil model, associating k_1 as with a rapidly decaying (labile) carbon pool and k_3 as a stable (recalcitrant) carbon pool. Inputs from litterfall rates (L_{VP}, L_{ML}, L_T) or root turnover (δ_RC_R) enter a different soil carbon pool based on the assumed lability of the carbon. The quasi-steady dynamics for the Quality submodel are shown in Equation 2.6:

$$\begin{aligned} R_A &= \frac{g_R}{g_R+\delta_R}(\alpha-\beta)F_{GPP} \\ C_1^* &= \frac{\beta F_{GPP} + L_{VP}}{k_1+r_1} \\ C_2^* &= \frac{1}{k_2+r_2}\left(L_{ML} + \frac{\delta_R}{g_R+\delta_R}(\alpha-\beta)F_{GPP} + r_1C_1^*\right) \\ C_3^* &= \frac{L_T + r_2C_2^*}{k_3} \\ R_H &= (1-\epsilon)\left(k_1C_1^* + k_2C_2^* + k_3C_3^*\right) \\ R_G &= \epsilon\left(k_1C_1^* + k_2C_2^* + k_3C_3^*\right) \\ R_S &= R_A + R_H + R_G \end{aligned} \tag{2.6}$$

In Equation 2.6, expressions for C_1^*, C_2^*, and C_3^* are for ease of model presentation, but also represent the quasi-steady values for the soil carbon pools C_1, C_2, and C_3, respectively. The FireGrow model was applied at each of the different sites (2012, 1990, 1968, and Control), soil depths (5 or 10 cm), or submodels (Null, Microbe, Quality), resulting in 24 different model outputs of soil respiration fluxes (R_A, R_H, R_G, and R_S).

2.4. Model parameterization

Parameter values for each of the different submodels are shown in Table 1. Parameter values were (1) taken from literature (α, β, k_1, k_2, k_3), (2) previously estimated and determined as well-constrained in

https://doi.org/10.1017/eds.2026.10034 Published online by Cambridge University Press

Zobitz et al. (2021) ($Q_{10,R}$), or (3) estimated directly with the MCMC parameter estimation technique (described below) (Richey, 2010; Zobitz et al., 2011; Blitzstein and Hwang, 2019). For this MCMC optimization, we selected litterfall rates (L_{VP}, L_{ML}, and L_T), root turnover (δ_R), kinetic root rate constant (k_R), or microbial processes (ϵ, r_1, r_2) as parameters for optimization. We selected these parameters based on their functional relationship to soil respiration, as defined in Equations 2.4–2.6, and because they were previously identified as poorly constrained (Zobitz et al., 2021).

The MCMC technique estimates parameters for each chronosequence site (2012, 1990, 1968, or Control), soil depth (5 or 10 cm), and model (Null, Microbe, or Quality). Briefly, this algorithm iteratively explores the prescribed parameter space that minimizes the log-likelihood function (Equation 2.7) between measured and modeled median soil respiration in August 2015 (when we collected field measurements):

$$\ln\left(L\left(\vec{\alpha}|\vec{x},\vec{y}\right)\right) = N\ln\left(\frac{1}{\sqrt{2\pi}\sigma}\right) - \sum_{i=1}^{N}\frac{\left(R_{S,meas}-R_{S,mod}\right)^2}{2\sigma^2}, \tag{2.7}$$

where N is the number of data points, $R_{S,meas}$ is the measured soil respiration, and $R_{S,mod}$ the modeled soil respiration (Equations 2.4, 2.5, and 2.6). Each chronosequence site had three values of $R_{S,meas}$; we computed the median of modeled R_S in August 2015 for the corresponding value of $R_{S,mod}$. The value of σ was set to 0.86 gC m^{-2} d^{-1}, the computed standard deviation of $R_{S,meas}$ across all chronosequence sites.

The MCMC technique implements the Metropolis-Hastings algorithm (Metropolis et al., 1953). Given a random set of initial parameter values, the algorithm selects a single parameter, changing its value by a random amount, and evaluates the log-likelihood with this proposed (new) parameter set. This parameter set is accepted when the log-likelihood decreases, or with a probability proportional to the difference of the log-likelihoods.

Two additional steps are used to accelerate convergence to the assumed optimum value of the log-likelihood. First, we used simulated annealing (Eglese, 1990) to tune the allowed uniform parameter range of values as the optimization progresses. Second, we initially ran multiple parallel chains with different initial starting points. After a specified number of iterations, the chain with the smallest log-likelihood value is selected for an additional number of iterations and no simulated annealing. The set of accepted parameters from this final phase characterizes the posterior parameter distribution and modeled respiration outputs. For both simulated annealing phases, we set the number of iterations to be 1000 for an initial exploration of the parameter space, and the final estimation phase at 2000 iterations.

Once the parameter optimization is completed, we use the set of accepted parameter values from the final estimation phase to calculate (1) the annual cumulative flux for each year spanning 2016–2022 and (2) an ensemble average of the annual cycle of R_S and its components from 1 January 2016 to 31 December 2022. For both calculations, we report the median and 50% centered confidence interval. We selected the 50% confidence interval rather than a standard deviation to conservatively compensate for the usage of the derived data (Section 2.2).

2.5. Empirical evaluation of modeled outputs

To further corroborate our modeled results, we used three previously established empirical relationships between soil respiration components and cumulative litterfall, represented here as the sum of living tree litter (L_T), vascular plants litter (L_{VP}), and moss and lichen litter (L_{ML}). The litterfall rates were all estimated by our parameter optimization method. While Equations 2.4–2.6 describe functional relationships between respiration components to estimated parameters, we do not a priori assume these empirical relationships.

We applied three previously established empirical relationships linking soil respiration components to cumulative litterfall. First, Davidson et al. (2002), through a meta-analysis of annual soil respiration and litterfall using data from published studies and the AmeriFlux network, showed that total soil respiration (R_S) is linearly related to cumulative annual litterfall. Second, Bond-Lamberty et al. (2004b) and Bond-

https://doi.org/10.1017/eds.2026.10034 Published online by Cambridge University Press

Lamberty and Thomson (2010) established a log–log relationship between heterotrophic respiration (R_H) and total soil respiration, based on data compiled from published studies and the Global Soil Respiration Database. Third, Subke et al. (2006) used field and laboratory studies to derive a logarithmic relationship between the proportion of autotrophic respiration ($p_A = R_A/R_S$) and total soil respiration.

3. Results

Our key questions focus on the impacts of (1) site-specific variability for soil model parameterization and (2) model structure for predicted components of soil respiration. The factorial complexity of the model parameterization (four sites, three models, two depths) requires presentation of results across chronosequence sites, depth of the soil temperature measurement (5 or 10 cm), or soil carbon submodel. To evaluate our first key question, we analyzed the distributions of accepted parameters from our optimization method along with broad comparisons between measured and modeled R_S. For the second key question, we evaluated annual patterns of the predicted soil respiration and compared cumulative annual totals to empirical relationships previously established in the literature.

Figure 4 presents violin plots illustrating parameter estimates for each submodel (Null, Microbe, and Quality) and soil depth (5 cm and 10 cm) across the chronosequence sites (2012, 1990, 1968, and Control). Each subplot is scaled according to the minimum and maximum parameter values (Table 1), with dashed gridlines denoting quartile values for comparison across a row.

Several estimated parameters in Figure 4 varied systematically with chronosequence age. For example, estimates of L_{VP}, L_T, and L_{ML} increased with time since fire disturbance and decreased for the Control site. This pattern is consistent with greater observed litterfall accompanying biomass recovery (Köster et al., 2014; Aaltonen et al., 2019a). In contrast, other estimated parameters such as k_R and ϵ showed little sensitivity to chronosequence age, suggesting time since disturbance does not influence these parameters. Parameters such as r_1 and r_2 in the Quality submodel had different trends across the chronosequence depending on the soil temperature measurement depth used for model parameterization, demonstrating the sensitivity of parameter estimates to input data.

Table 2 summarizes statistics from the posterior log-likelihood distributions by model, chronosequence site, and soil depth. At both 5 and 10 cm depths, the 1968 site showed the broadest distributions, as reflected in higher standard deviations, suggesting greater variation in soil respiration components at this site. Figures 4 and 5 in the Supplementary Information displays the trajectory of the log-likelihood ($ln(L)$, Equation 2.7) as the MCMC parameter estimation technique progresses.

Using the accepted sets of parameter values from Figure 4, we conducted forward simulations for each model and computed soil respiration fluxes at all chronosequence sites and soil depths. Figure 5 compares measured soil respiration ($R_{S,meas}$; median values from replicate plots at each site) to modeled soil respiration ($R_{S,mod}$; median simulated values during August when field measurements were collected). The joint violin plots in Figure 5 illustrate the distributions of $R_{S,mod}$ and $R_{S,meas}$, while the reported R^2 values quantify the correspondence between modeled and measured fluxes.

Overall, the variability in $R_{S,meas}$ increased with chronosequence age, as indicated by the widening of the violins across panels, whereas the range of $R_{S,mod}$ remained relatively consistent among models and sites (violins approximately have the same height). Although modeled and measured fluxes generally clustered near the 1:1 line, $R_{S,mod}$ tended to underestimate $R_{S,meas}$ at the 1968 site and overestimate it at the 2012 site. This consistent pattern across all submodel types (Null, Microbe, and Quality) suggests a bias in the formulation of R_A (represented as Equation 2.1 for all submodels). The moderate R^2 values (0.50–0.56) indicate that additional processes not represented in any submodel structure may also influence R_S. We discuss this further in Section 4.3.

With the FireGrow submodel evaluations, at each chronosequence site, depth of soil temperature measurement, and submodel, we summarized the annual cycle from 1 January 2016 to 31 December 2022 as an ensemble average, computing the median and 50% centered confidence interval (Figure 6). All submodels replicated an expected seasonal annual cycle (independent of depth), albeit with wider confidence intervals for the Quality model. In Table 2 of the Supplementary Information, we report the

https://doi.org/10.1017/eds.2026.10034 Published online by Cambridge University Press

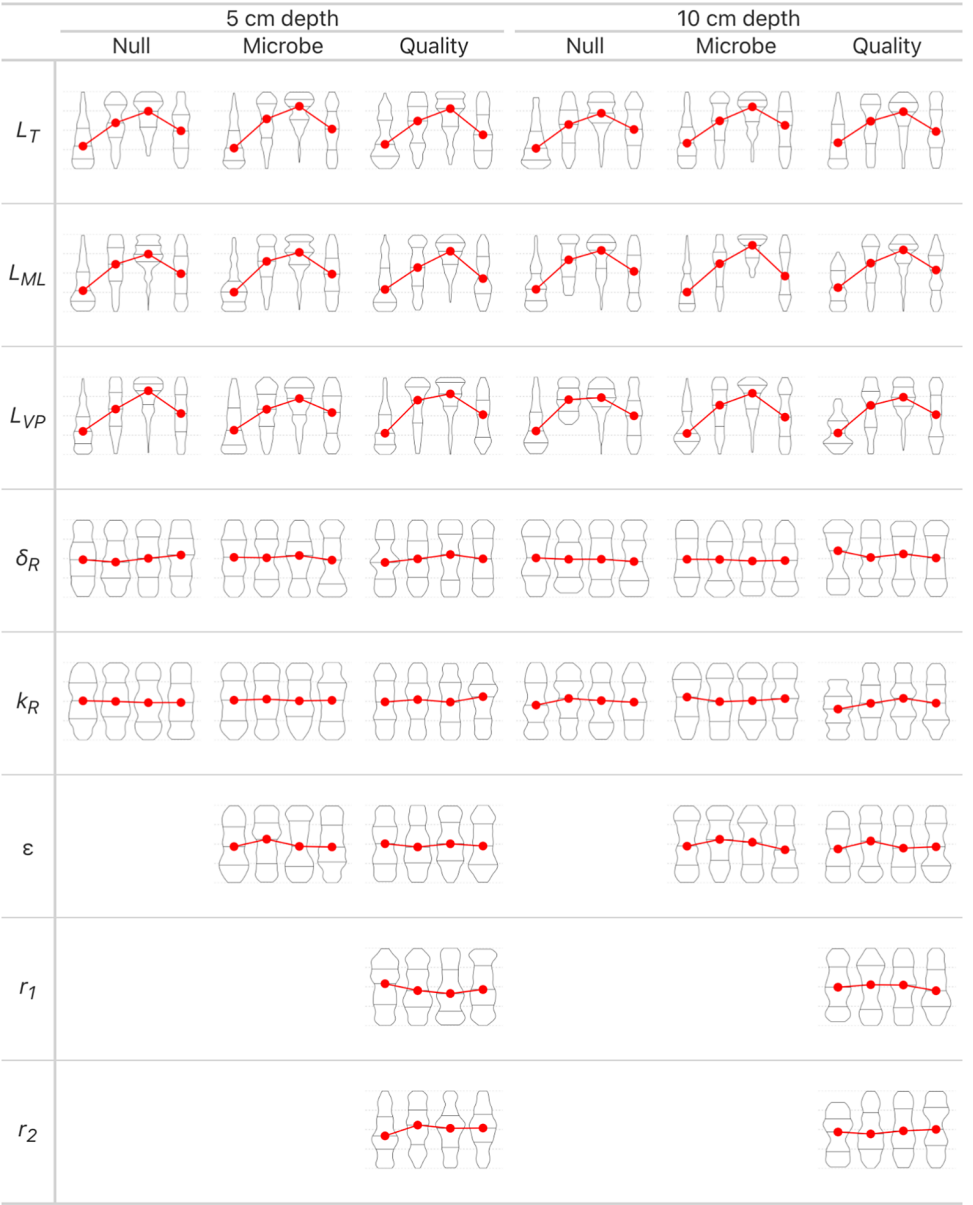


Figure 4. *Violin distributions from parameter estimation for different submodels (Null, Microbe, and Quality), parameterized with soil respiration at 5 cm depth (left three columns) or 10 cm depth (right three columns). For each subplot, the horizontal axis is arranged by year of fire disturbance (2012, 1990, 1968, or Control), and the vertical axis is scaled according to the minimum and maximum values of the parameter estimates in Table 1, with dashed gridlines representing quartiles (consistent across each row). The red line in each violin plot connects the median estimated value of each parameter across the chronosequence.*

median and 50% centered confidence intervals for annual litterfall inputs or fluxes from the results shown in Figure 6.

Similarly, Figure 7 presents p_A together with the proportion of R_G to R_S and R_H to R_S (denoted as p_G, and p_H, respectively) for each model and chronosequence site. Periods without data (approximately

https://doi.org/10.1017/eds.2026.10034 Published online by Cambridge University Press

Table 2. *Statistics from the posterior log-likelihood function ($\ln(L)$) from the MCMC parameter estimation method at each chronosequence site and FireGrow submodel*

Depth (cm)	Model	$\ln(L)$ statistic	2012	1990	1968	Control
5 cm	Null	Median	2.70	2.61	3.06	3.39
5 cm	Null	Maximum	5.25	4.42	5.62	4.65
5 cm	Null	Standard deviation	5.25	4.42	5.62	4.65
5 cm	Microbe	Median	2.67	2.61	3.16	3.39
5 cm	Microbe	Maximum	4.42	4.92	6.01	4.51
5 cm	Microbe	Standard deviation	4.42	4.92	6.01	4.51
5 cm	Quality	Median	2.65	2.59	3.14	3.39
5 cm	Quality	Maximum	5.31	4.81	5.71	4.44
5 cm	Quality	Standard deviation	5.31	4.81	5.71	4.44
10 cm	Null	Median	2.68	2.62	3.13	3.38
10 cm	Null	Maximum	5.02	4.62	7.60	4.46
10 cm	Null	Standard deviation	5.02	4.62	7.60	4.46
10 cm	Microbe	Median	2.64	2.59	3.19	3.38
10 cm	Microbe	Maximum	5.97	4.14	7.82	4.52
10 cm	Microbe	Standard deviation	5.97	4.14	7.82	4.52
10 cm	Quality	Median	2.67	2.63	3.14	3.39
10 cm	Quality	Maximum	4.18	4.73	6.77	4.76
10 cm	Quality	Standard deviation	4.18	4.73	6.77	4.76

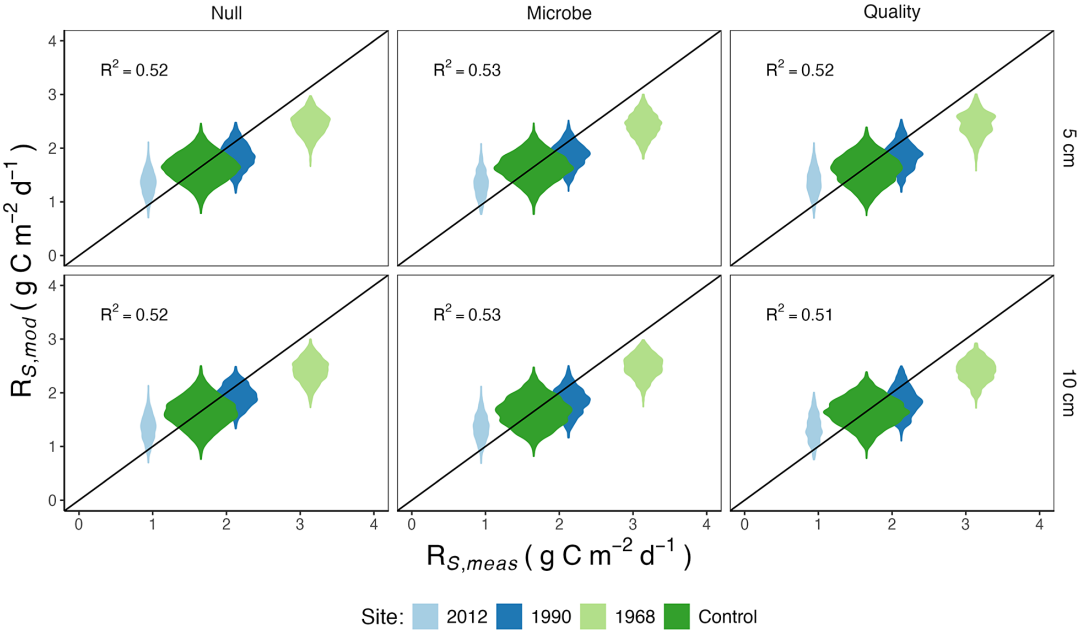


Figure 5. *Comparison between measured soil respiration ($R_{S,meas}$) to modeled soil respiration ($R_{S,mod}$) from FireGrow submodel evaluation using sets of accepted parameter values from MCMC optimization. Values of $R_{S,meas}$ are computed as the median within each replicate plot at each chronosequence site, shown as a violin plot to indicate the distribution of $R_{S,meas}$. Values of $R_{S,mod}$ are computed as the median values of R_S in August when field measurements occurred. R^2 values for each regression are displayed on the subplot.*

https://doi.org/10.1017/eds.2026.10034 Published online by Cambridge University Press

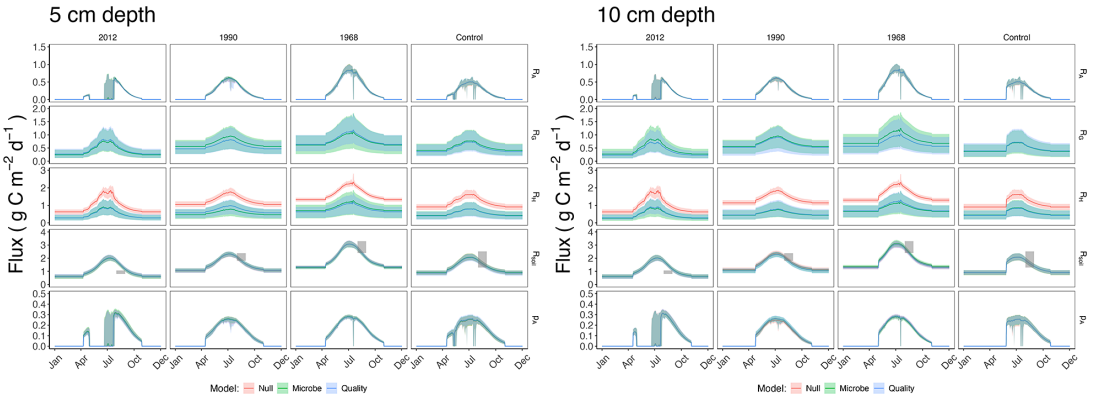


Figure 6. *Forward model evaluation results of summarized annual timeseries, along with the 50% centered confidence interval for each of the submodels (Null, Microbe, and Quality) and depth of soil temperature measurements (5 or 10 cm). The ensemble average was computed from model results from 1 January 2016 to 31 December 2022 generated from all sets of accepted parameter values. Soil respiration fluxes are reported in gC m^{-2} d^{-1}. R_A: autotrophic respiration; R_G: microbial growth respiration; R_H: microbial maintenance respiration; R_S: total soil respiration $(=R_A+R_G+R_H)$; and $p_A=R_A/R_S$ (unitless).*

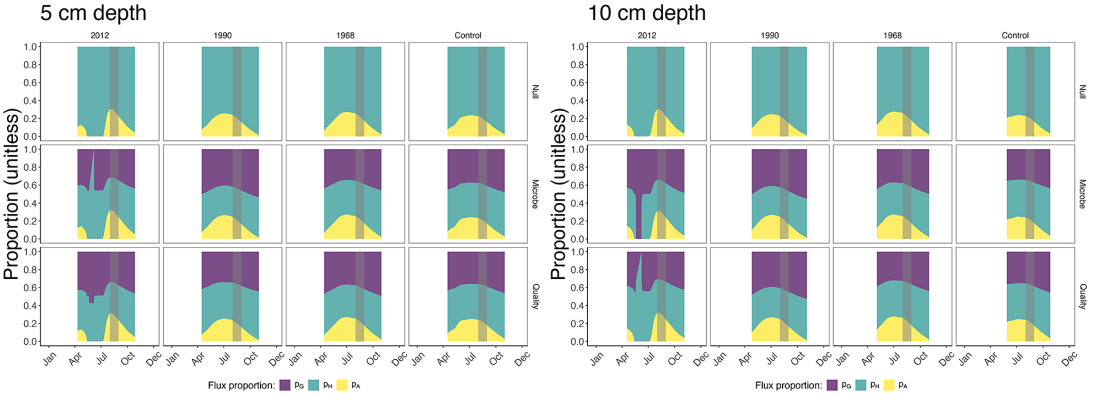


Figure 7. *Forward model results of the annual proportion of components of soil respiration for each of the submodels (Null, Microbe, and Quality) and depth of soil temperature measurements (5 or 10 cm). Proportions were computed with soil respiration using the median values from Figure 6. p_A: proportion of autotrophic respiration (yellow); p_G: proportion of heterotrophic growth respiration (purple); p_H: proportion of heterotrophic maintenance respiration (blue). We assume p_A is zero in freezing soils, so results are only shown when $p_A>0$, considered to be the active growing season (approximately April–October).*

January–April and October–December) correspond to when soils are frozen, during which we assume that R_A equals zero. Computing p_A provides a standardized measure that facilitates cross-site comparisons of respiration partitioning with other ecosystems (Jian et al., 2022b), which we discuss in Section 4.2.

Notably, the annual pattern in R_A and p_A in Figures 6 and 7 for the 2012 chronosequence site displayed a longer period during which R_A and p_A remained near zero before reaching a seasonal peak. This pattern is consistent with the environmental inputs of *SWC* and F_{GPP} (Figure 2), which directly influence R_A through g_R (Equation 2.2, driven by *SWC*) and F_{GPP} (Equation 2.1). At the 2012 site, F_{GPP} was lower overall, and in early summer *SWC* declined to zero, thereby suppressing R_A and p_A.

https://doi.org/10.1017/eds.2026.10034 Published online by Cambridge University Press

A factor influencing R_A (and by association p_A) at all sites is the function $h(SWC)$ (Equation 2.2; Moyano et al. [2013]). This function reaches an optimum near unity when $SWC = 0.64$, and decreases when $SWC > 0.64$, thereby reducing R_A. In early spring at the 1990, 1968, and Control sites, SWC remains closer to this optimum (Figure 2), which helps explain higher R_A values during that period. Additionally, to verify that our implementation of $h(SWC)$ did not unduly influence these patterns, we repeated the parameter estimation with $h(SWC) = 1$ and $h(SWC) = SWC$. The resulting model outputs are shown in Figures 6 and 7 of the Supplementary Information exhibited no early-season suppression of R_A (and by association p_A) at the 2012 site, while the overall seasonal patterns remained consistent.

To independently corroborate our parameter estimates and model results, we used submodel evaluations to compute the distribution of annual cumulative litterfall ($= L_T + L_{VP} + L_{ML}$) and total annual soil carbon fluxes and their components (Table 2 in the Supplementary Information). We then compared these outputs against three empirical relationships established in the literature: (1) annual litterfall versus total soil respiration (R_S) (Davidson et al., 2002), (2) heterotrophic respiration (R_H) versus total soil respiration (Bond-Lamberty et al., 2004b), and (3) autotrophic respiration proportion (p_A) versus total soil respiration (Subke et al., 2006). We also evaluated linear regression statistics from the modeled results for each relationship (Figure 8).

In Figure 8a, all models showed strong visual agreement with the empirical relationship established by Davidson et al. (2002) ($R_S = 161 + 3.61 L_T$). This visual agreement was supported by simple linear regression, which indicated significant associations across all submodels and depths ($p < .05$). The Microbe submodel at 10 cm depth exhibited the lowest regression RMSE among all models (71 g C m^{-2} yr^{-1}).

For Figure 8b, the Null submodel overestimated R_H relative to the expected empirical relationship ($\ln(R_H) = 0.22 + 0.87 \ln(R_S)$; Bond-Lamberty et al. (2004b), Bond-Lamberty and Thomson [2010]). This overestimation likely occurs because the Null submodel does not separate heterotrophic respiration into R_G and R_H, whereas the Microbe and Quality submodels separately describe R_G and R_H (Equations 2.5 and 2.6, respectively). Linear regression indicated that most submodels and depths were significantly associated ($p < .05$), except for the Quality model at 5 cm depth. The Microbe submodel at 10 cm depth again had the lowest regression RMSE (1.1 g C m^{-2} yr^{-1} at 5 cm depth after converting from $\ln(R_H)$ to R_H).

Finally, Figure 8c shows that all models underestimated p_A relative to the expected empirical relationship ($p_A = -0.482 + 0.138 \ln(R_S)$; Subke et al. [2006]). This outcome is consistent with the absence of significant associations between $\ln(R_H)$ and p_A for any submodel or depth. RMSE values for all submodels ranged from 0.32 to 0.33.

4. Discussion

The objective of this study was to model and characterize annual patterns of soil respiration components across a fire chronosequence. Measuring soil respiration with chamber-based methods or the flux-gradient approach is inherently challenging (Maier and Schack-Kirchner, 2014), and even more so for the remote sites in this study. The remoteness and access to our sites confined the period of data collection to one month, which we compensated for using a factorial design approach (4 sites, 3 models, 2 depths) for model analysis and evaluation.

All submodels produced annual patterns of soil respiration (and their associated components) across the fire chronosequence (Figures 6 and 7). We used the median for parameter optimization and modeled fluxes because it reduces the influence of outliers (Devore et al., 2021) and intra-site variation, improving comparability across the chronosequence. After evaluating the parameter estimation method, we examine how chronosequence site and submodel structure influence model parameterization and outputs. Finally, we assess the extent to which the Microbe and Quality submodels better replicate modeled components of soil respiration compared to the Null submodel.

https://doi.org/10.1017/eds.2026.10034 Published online by Cambridge University Press

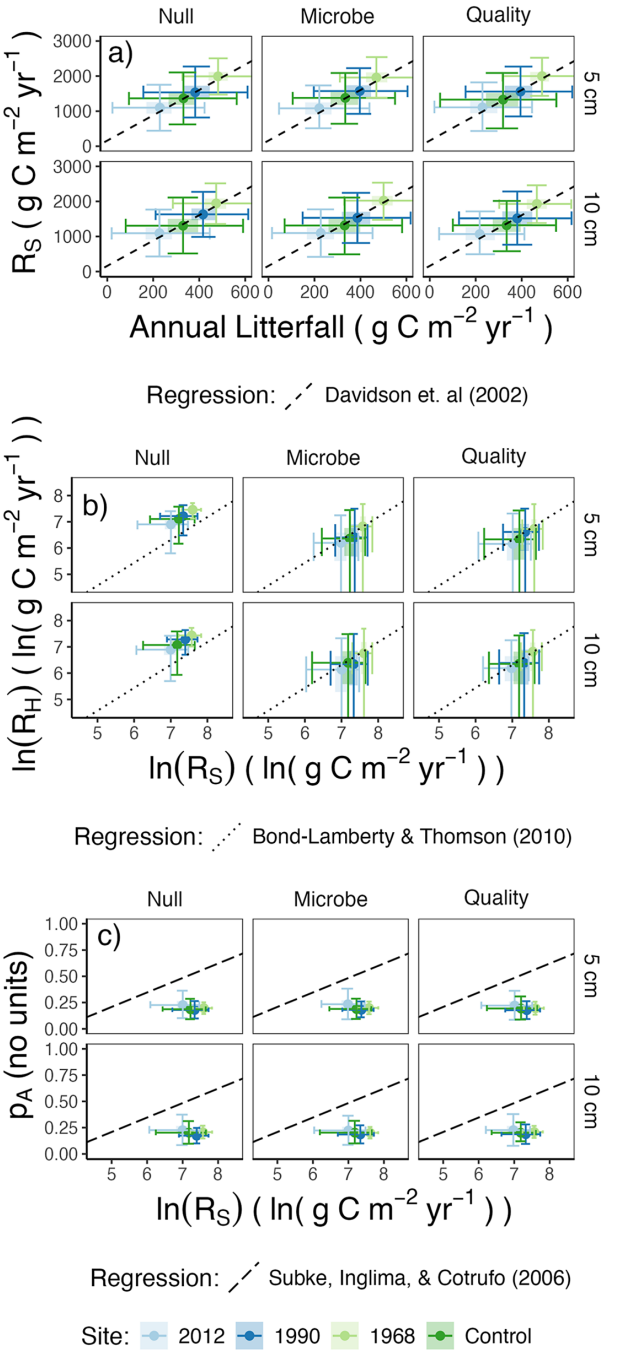


Figure 8. *Associations between annual soil respiration components, cumulative litterfall, and the proportion of autotrophic respiration compared to parameterization at either the 5 cm or 10 cm depth and the soil carbon submodel studied. For each scatterplot, boxes represent the 25–75% distribution of a covariate, and whiskers represent the minimum or maximum of a measurement, with points representing the median value, as reported in the Supplementary Information. Since R_A is zero for freezing soils, values of p_A are computed during the active growing season (approximately April–October). For comparison, previously reported empirical relationships are represented. (a): $R_S = 161 + 3.61L_T$, Davidson et al. (2002); (b): $\ln(R_H) = 0.22 + 0.87\ln(R_S)$, Bond-Lamberty et al. (2004b) and Bond-Lamberty and Thomson (2010); (c): $p_A = -0.482 + 0.138\ln(R_S)$, Subke et al. (2006).*

https://doi.org/10.1017/eds.2026.10034 Published online by Cambridge University Press

4.1. Evaluation of modeling approach and parameter estimation method

We applied a quasi-steady-state assumption to derive empirical equations for respiration fluxes (R_A, R_H, and R_G), enabling direct identification of parameters influencing soil respiration (Equations 2.4–2.6). This assumption reduces model complexity (Carvalhais et al., 2008; Todd-Brown et al., 2012; Ryan et al., 2018) and computational bottlenecks (Xia et al., 2012; Fang et al., 2014; Fer et al., 2018; Wiltshire et al., 2023), making sensitivity analyses more tractable (Figures 4–7), especially for the multiple sites and models analyzed in this study.

Dynamic process models (Sacks et al., 2006; Zobitz et al., 2008) require explicit representation of carbon pools (C_S, C_R, C_M, and C_A); parameter estimation with these process models are best constrained with repeated measurements of root, soil, or microbial stocks. As such observations were unavailable for this study, the quasi–steady-state approach we adopted is a compromise between data availability and model complexity. Nevertheless, incorporating measured carbon stock data in future work could help reduce parameter uncertainty and improve model-data comparisons (Richardson et al., 2010).

Despite these limitations, the MCMC method effectively characterized the posterior likelihood distribution at all sites and models (Table 2 and Figures 4 and 5 in the Supplementary Information), with the widest posterior distribution at the 1968 chronosequence site, also reflected as the site with the widest violin plot (Figure 5). The depth at which soil temperature was measured did not meaningfully impact the parameter estimation and consequently the annual cycle of soil respiration components (Figures 6 and 7).

Although we sought to maximize the information content of the field measurements, the limited number of observations at each chronosequence site constrains the extent to which the model results in Figure 6 can be generalized. In this context, the estimated parameters should be viewed as (1) guiding intuition for model behavior, (2) identifying constraints on the model structure, and (3) evaluating whether parameter ranges narrower than those summarized in Table 1 are supported by the data. Future applications incorporating longer time series or repeated seasonal sampling into the MCMC framework would enable more robust evaluation of the model (Braswell et al., 2005), perhaps with increased computational cost.

4.2. Chronosequence effects on parameterization and model results

A key question of this study was to examine the sensitivity of model parameters to time since fire disturbance or chronosequence age. One approach to evaluate associations between chronosequence site and model parameters is through investigation of the distribution of accepted parameter values using chronosequence age as a covariate (Figure 4). Chronosequence age strongly influenced parameters related to litterfall rates (L_T, L_{VP}, L_{ML}). In contrast, root turnover (δ_R) showed little sensitivity to age, despite playing a similar functional role in increasing soil carbon substrate (Figure 3). The r_1 and r_2 parameters in the Quality submodel showed different trends across the chronosequence depending on the soil temperature measurement depth. However, this sensitivity did not meaningfully affect model–data agreement (Figure 5) or comparisons to empirical patterns in respiration components (Figures 8b–c). Other Microbe and Quality submodel parameters showed little sensitivity to chronosequence age.

We found significant association between inferred annual litterfall rates to soil respiration consistent with previously established empirical patterns between litterfall rates and respiration (Figure 8a; Davidson et al. [2002]). The sensitivity of litterfall rates with soil respiration (and therefore chronosequence age) also conforms with expectations from observational studies. Soil respiration and litterfall rates are directly associated with each other (Reynolds and Hunter, 2001; Subke et al., 2004; Wei and Man, 2021; Paré et al., 2022). These litterfall rates also increase following recovery from fire disturbance (Grigal and McColl, 1975).

Parameter estimates of δ_R were not sensitive to chronosequence age (Figure 4), which was contrary to our expectations for three reasons. First, previous investigations at these same sites reported associations between soil moisture, root biomass, and time since the fire occurred (Aaltonen et al., 2019a, 2019b). Second, previous studies have established links between root turnover and soil respiration. Adamczyk et al. (2021) found that root exudates are positively associated with microbial abundance and diversity,

https://doi.org/10.1017/eds.2026.10034 Published online by Cambridge University Press

and coincidentally impact overall soil respiration. Similarly, Finér et al. (2011) showed that fine root biomass can be sensitive to temperature, soil moisture, or either environmental factors. Third, root turnover ($\delta_R C_R$; dashed line in ROOTS, Figure 3; Equation 5.2, Supplementary Information) and root exudation (βF_{GPP}, Equation 5.4, Supplementary Information) transfer carbon from the root pool to the soil pool. Root turnover and exudation appear in the quasi-steady state expression for R_A (Equation 2.1). Given these connections among disturbance history, root activity, and model representation of δ_R, we would have expected δ_R to vary across the chronosequence.

This insensitivity in δ_R is a contributing factor for the weak association between modeled p_A and observed $\ln(R_S)$ (Figure 8c). Our modeled p_A values were lower than those predicted by the empirical relationship from Subke et al. (2006). Similarly, Jian et al. (2022b), in a global synthesis study from the Soil Respiration Database (SRDB), reported p_A to range 0.42 ± 0.18, without clear trends across ecosystem types. The reported range from Jian et al. (2022b) is within the uncertainty of p_A in Figure 8c and during the peak growing season in Figures 6 and 7. Overall, these findings suggest our submodels oversimplify root carbon dynamics.

We anticipate that the additional data collection—focused on better understanding of δ_R—would feed forward into model refinement and improvement. Systematic surveys of root biomass during different periods in the year could help elucidate which environmental factors (e.g. *GPP* or *NPP*) (Ruess et al., 2003) facilitate root growth, exudation, and turnover at particular chronosequence sites. With that information, models of root exudates could be time-dependent or associated with environmental forcing variables.

Model refinement of root turnover would have secondary impacts on p_A. The quasi-steady state expressions formulated for the FireGrow model establish direct relationships between model outputs (R_A, R_G, and R_H) and model parameters. In Equation 2.1, R_A, and hence p_A increases when δ_R decreases. Model improvement for the structural consideration of root carbon dynamics should also consider uncertainties in the association between between p_A and R_S. Jian et al. (2022b) also concluded that R_S explains 2% of the variability on p_A. Given the methodological challenges of direct measurement of p_A (Hanson et al., 2000), uncertainty reduction in model estimates of p_A could occur through (1) inferring root turnover rates from measurable aboveground indicators (such as aboveground leaf or needle turnover rates [Sloan et al., 2013]); or (2) separation of different root classes (e.g. fine roots versus coarse roots [Kalyn and Van Rees, 2006; Finér et al., 2011; Neumann et al., 2020].

4.3. Structured models of soil carbon better replicate modeled components of soil respiration

Figures 6 and 7 do not suggest any meaningful submodel differences between parameterization depth (5 or 10 cm). We also did not find any meaningful differences between different implementations of $h(SWC)$ beyond Equation 2.2 (see Supplementary Information). The lack of sensitivity to parameterization depth was unexpected, given the depth-specific differences in $Q_{10,R}$ (Table 1), but was likely offset by similar temperature profiles across depths at all chronosequence sites (Figure 2). The largest temperature gradient between depths (approximately 2 °C) occurred in midsummer at the Control site, though its effect on modeled respiration was likely marginal. We attribute this pattern to ground cover re-insulation, which reduces active layer thickness and steepens the soil temperature gradient (Köster et al., 2017; Aaltonen et al., 2019a, 2019b).

In Figure 6, the Null submodel consistently overestimates R_H across daily (and consequently) annual timescales; we attribute this overestimation to its formulation (Equation 2.4) that does not separately represent R_G and R_H. This overestimation is further reflected in the weaker empirical association between R_H and R_S (Figure 7b), compared to the Microbe and Quality submodels. In contrast, the Microbe and Quality submodels show broadly similar performance (Figures 6, 7), even though they differ in their representations of R_G and R_H (Equations 2.5 and 2.6). These results indicate that explicitly incorporating microbial processes provides a more accurate characterization of soil respiration components, even if structural differences among submodels produce comparable outcomes. While untested here, relaxing the quasi–steady-state assumption may further distinguish the Microbe and Quality submodels, but doing so would require additional observations of pool sizes or inferring litterfall rates from measured litterfall as previously discussed.

https://doi.org/10.1017/eds.2026.10034 Published online by Cambridge University Press

While model structure and microbial representation explain part of the variability in R_H, external site factors, such as fire history, also influence soil respiration dynamics. Kelly et al. (2021) identified autotrophic respiration and nutrient pulses following fire disturbances as key drivers of soil respiration. While fire intensity is also an important factor influencing post-fire soil dynamics (Ribeiro-Kumara et al., 2020; Kelly et al., 2021), all our sites experienced a stand-replacing fire, which we assume to be of equal fire intensity. Differences in fire severity or burn conditions across chronosequence sites could contribute to some of the observed variation in soil respiration rates; future work could elucidate the relative contributions of burn severity and time since disturbance to measured soil respiration.

Incorporating soil microbial processes into soil models can improve model–data agreement for soil respiration (Wutzler and Reichstein, 2013; Taş et al., 2014; Woolf and Lehmann, 2019; Pierson et al., 2022). Neglecting these dynamics or not including microbial interactions with soil carbon may lead to underestimation of projected climate responses, particularly in permafrost regions (Fan et al., 2013; Perveen et al., 2014; Keuper et al., 2020). Additional factors, such as long-term shifts in microbial community composition due to the presence or absence of snow cover (Männistö et al., 2018), may further influence respiration patterns. Iterative model refinement at affected sites may require seasonal parameter adjustments (Sacks et al., 2006; Zobitz et al., 2008) or explicit representation of frozen and thawed carbon pools (Schaefer and Jafarov, 2016). These microbial processes interact with the physical and structural characteristics of soils, highlighting the need to consider both abiotic and biotic factors when modeling soil respiration.

The interactions between climatic variables and the physical and structural characteristics of soil carbon are critical for understanding site-to-site differences in soil respiration (Luo et al., 2019; Paré et al., 2022). Among the driver variables used in our models, *GPP* and soil water content had the largest site-to-site variability (Figure 2). In Arctic permafrost ecosystems, winter–spring (and associated freeze/thaw cycles) can contribute as much as 5–20% to annual soil respiration (Mikan et al., 2002; Kurganova et al., 2007; Wang et al., 2014; Keuper et al., 2020). Although not explicitly tested in this study, we anticipate that freeze–thaw cycles stimulate soil heterotrophic respiration by mobilizing a thawed, highly labile soil carbon pool. These transient dynamics likely influence annual patterns of soil organic carbon accumulation, particularly in regions with short growing seasons constrained by permafrost dynamics and frozen soils. Direct field measurement of R_S during these spring periods (with subsequent model parameterization) could reduce uncertainty in modeled soil respiration components, offer alternative parameterizations, and improve agreement between measured and modeled $R_{S,meas}$ and $R_{S,mod}$ (Figure 5).

5. Conclusion

This study evaluated the ability to parameterize soil respiration models with differing representations of microbial dynamics across a fire chronosequence. All three model variants reproduced expected annual patterns of total soil respiration (R_S) consistent with time since fire disturbance. Parameter estimates were generally insensitive to soil depth (5 or 10 cm), indicating that depth had a limited effect on model parameter estimates and modeled soil respiration components. However, models that explicitly represented microbial carbon processes produced stronger model-data comparisons when evaluated against previously established empirical relationships. For our fire chronosequence sites, separate consideration of microbial processes compared to a bulk soil carbon pool is critical to accurately represent microbial contributions to soil carbon cycling; we expect that these findings generalize to other ecosystems. Additionally, parameters associated with aboveground litter inputs displayed variation with chronosequence site, generally consistent with previously observed patterns of vegetation recovery following fire disturbance.

Our results demonstrate that satellite-derived gross primary productivity (F_{GPP}), soil temperature (T_S), and soil water content (SWC) can serve as useful substitutes for direct field measurements in modeling soil respiration at remote or data-sparse ecosystems. Based on these findings, we offer three recommendations for future model development and data collection. First, direct field measurements of litterfall and more importantly root turnover rates would reduce model uncertainty by constraining other soil respiration parameters and improving model–data comparisons. Second, targeted sampling during seasonal transition periods (e.g., freeze–thaw cycles) would provide valuable constraints on root turnover and exudation,

https://doi.org/10.1017/eds.2026.10034 Published online by Cambridge University Press

microbial activity, and respiration dynamics. Third, future versions of the FireGrow model should relax the quasi–steady-state assumption, allowing for explicit coupling between microbial and soil carbon pools and environmental drivers that vary dynamically over the growing season. Future development of soil respiration models will benefit from explicit microbial carbon representation combined with field-based estimates of litterfall and root turnover rates, given that these inputs modulate substrate supply and often serve as a primary control on soil heterotrophic respiration.

Open peer review. To view the open peer review materials for this article, please visit http://doi.org/10.1017/eds.2026.10034.

Supplementary material. The supplementary material for this article can be found at http://doi.org/10.1017/eds.2026.10034.

Acknowledgements. We would like the thank feedback from two anonymous reviewers to improve the manuscript. Following initial revisions, select sentences of the text were refined with the assistance of Generative AI to enhance readability. Co-author Zobitz acknowledges B. S. Chelton for helpful discussion on this manuscript.

Author contribution. Conceptualization: J.Z. Methodology: J.Z. (modeling); J.P.; K.K.; F.B. (field data) Software: J.Z. Validation: J.Z. Formal Analysis: J.Z.; F.B. Investigation: J.Z. (modeling); J.P.; K.K.; F.B. (field data); X.Z. (data collection); H.A.; E.K. (experiment, data collection) Data curation: J.Z. Writing – original draft: J.Z. Writing – review and editing: F.B.; K.K.; E.K. Visualization: J.Z. Supervision: J.Z. Project Administration: J.Z. Funding Acquisition: J.Z. (Fulbright).

Competing interests. The authors declare no competing interests.

Data availability statement. The data and R scripts used to execute/report on the analyses in the paper can be found at https://github.com/jmzobitz/FireGrow, and are preserved at https://zenodo.org/doi/10.5281/zenodo.11493787 via Zenodo.

Ethics statement. The research meets all ethical guidelines, including adherence to the legal requirements of the study country.

Funding statement. Co-author Zobitz was funded by the Fulbright Finland Foundation and Saastamoinen Foundation Grant in Health and Environmental Sciences. This work was funded by the Academy of Finland (project numbers 286685, 294600, 307222, 327198, and 337550). Travel funding was provided from EU InterAct (H2020 Grant Agreement No. 730938).

References

Aaltonen H, **Köster K**, **Köster E**, **Berninger F**, **Zhou X**, **Karhu K**, **Biasi C**, **Bruckman V**, **Palviainen M and Pumpanen J** (2019a) Forest fires in Canadian permafrost region: The combined effects of fire and permafrost dynamics on soil organic matter quality. *Biogeochemistry 143*(2), 257–274.

Aaltonen H, **Palviainen M**, **Zhou X**, **Köster E**, **Berninger F**, **Pumpanen J and Köster K** (2019b) Temperature sensitivity of soil organic matter decomposition after forest fire in Canadian permafrost region. *Journal of Environmental Management 241*, 637–644.

Adamczyk M, **Rüthi J and Frey B** (2021) Root exudates increase soil respiration and alter microbial community structure in alpine permafrost and active layer soils. *Environmental Microbiology 23*(4), 2152–2168.

Allison SD (2012) A trait-based approach for modelling microbial litter decomposition. *Ecology Letters 15*(9), 1058–1070.

AppEEARS (2022). Application for Extracting and Exploring Analysis Ready Samples (AppEEARS). Version 3.4. Available at https://appeears.earthdatacloud.nasa.gov (accessed June 9, 2022).

Beven K and Freer J (2001) Equifinality, data assimilation, and uncertainty estimation in mechanistic modelling of complex environmental systems using the GLUE methodology. *Journal of Hydrology 249*(1–4), 11–29.

Blitzstein JK and Hwang J (2019) *Introduction to Probability*, 2nd Edn. Boca Raton: Chapman and Hall/CRC.

Bond-Lamberty B (2018) New techniques and data for understanding the global soil respiration flux. *Earth's Future 6*(9), 1176–1180.

Bond-Lamberty B and Thomson A (2010) A global database of soil respiration data. *Biogeosciences 7*(6), 1915–1926.

Bond-Lamberty B, **Wang C and Gower ST** (2004a) Contribution of root respiration to soil surface CO_2 flux in a boreal black spruce chronosequence. *Tree Physiology 24*(12), 1387–1395.

Bond-Lamberty B, **Wang C and Gower ST** (2004b) A global relationship between the heterotrophic and autotrophic components of soil respiration? *Global Change Biology 10*(10), 1756–1766.

Bosatta E and Ågren GI (1985) Theoretical analysis of decomposition of heterogeneous substrates. *Soil Biology and Biochemistry 17*(5), 601–610.

Bosatta E and Ågren GI (2002) Quality and irreversibility: Constraints on ecosystem development. *Proceedings of the Royal Society of London B 269*, 203–210.

Braswell BH, **Sacks WJ**, **Linder E and Schimel DS** (2005) Estimating diurnal to annual ecosystem parameters by synthesis of a carbon flux model with eddy covariance net ecosystem exchange observations. *Global Change Biology 11*(2), 335–355.

Burnham KP and Anderson DR (eds) (2002) *Model Selection and Multimodel Inference*. New York, NY: Springer New York.

Carvalhais N, **Reichstein M**, **Seixas J**, **Collatz GJ**, **Pereira JS**, **Berbigier P**, **Carrara A**, **Granier A**, **Montagnani L**, **Papale D**, **Rambal S**, **Sanz MJ and Valentini R** (2008) Implications of the carbon cycle steady state assumption for biogeochemical modeling performance and inverse parameter retrieval. *Global Biogeochemical Cycles 22*(2), GB2007.

Chen H and Tian H-Q (2005) Does a general temperature-dependent Q_{10} model of soil respiration exist at biome and global scale? *Journal of Integrative Plant Biology 47*(11), 1288–1302.

Davidson EA, **Belk E and Boone RD** (1998) Soil water content and temperature as independent or confounded factors controlling soil respiration in a temperate mixed hardwood forest. *Global Change Biology 4*(2), 217–227.

Davidson EA, **Janssens IA and Luo Y** (2006) On the variability of respiration in terrestrial ecosystems: Moving beyond Q10. *Global Change Biology 12*, 154–164.

Davidson EA, **Savage K**, **Bolstad P**, **Clark DA**, **Curtis PS**, **Ellsworth DS**, **Hanson PJ**, **Law BE**, **Luo Y**, **Pregitzer KS**, **Randolph JC and Zak D** (2002) Belowground carbon allocation in forests estimated from litterfall and IRGA-based soil respiration measurements. *Agricultural and Forest Meteorology 113*(1), 39–51.

Devore JL, **Berk KN and Carlton MA** (2021) *Modern Mathematical Statistics with Applications*, 3rd Edn., Springer Texts in Statistics. Cham, Switzerland: Springer International Publishing.

Eglese RW (1990) Simulated annealing: A tool for operational research. *European Journal of Operational Research 46*(3), 271–281.

Elzein A and Balesdent J (1995) Mechanistic simulation of vertical distribution of carbon concentrations and residence times in soils. *Soil Science Society of America Journal 59*(5), 1328–1335.

Famiglietti CA, **Smallman TL**, **Levine PA**, **Flack-Prain S**, **Quetin GR**, **Meyer V**, **Parazoo NC**, **Stettz SG**, **Yang Y**, **Bonal D**, **Bloom AA**, **Williams M and Konings AG** (2021) Optimal model complexity for terrestrial carbon cycle prediction. *Biogeosciences 18*(8), 2727–2754.

Fan Z, **Jastrow JD**, **Liang C**, **Matamala R and Miller RM** (2013) Priming effects in boreal Black spruce Forest soils: Quantitative evaluation and sensitivity analysis. *PLoS One 8*(10), e77880.

Fan N, **Koirala S**, **Reichstein M**, **Thurner M**, **Avitabile V**, **Santoro M**, **Ahrens B**, **Weber U and Carvalhais N** (2020) Apparent ecosystem carbon turnover time: Uncertainties and robust features. *Earth System Science Data 12*(4), 2517–2536.

Fang Y, **Liu C**, **Huang M**, **Li H and Leung LR** (2014) Steady state estimation of soil organic carbon using satellite-derived canopy leaf area index. *Journal of Advances in Modeling Earth Systems 6*(4), 1049–1064.

Fang C and Moncrieff JB (2001) The dependence of soil CO2 efflux on temperature. *Soil Biology and Biochemistry 33*(2), 155–165.

Fer I, **Kelly R**, **Moorcroft PR**, **Richardson AD**, **Cowdery EM and Dietze MC** (2018) Linking big models to big data: Efficient ecosystem model calibration through Bayesian model emulation. *Biogeosciences 15*(19), 5801–5830.

Ferraz de Almeida R, **Rodrigues Mikhael JE**, **Oliveira Franco F**, **Fonseca Santana LM and Wendling B** (2019) Measuring the labile and recalcitrant pools of carbon and nitrogen in forested and agricultural soils: A study under tropical conditions. *Forests 10*(7), 544.

Finér L, **Ohashi M**, **Noguchi K and Hirano Y** (2011) Factors causing variation in fine root biomass in forest ecosystems. *Forest Ecology and Management 261*(2), 265–277.

Friedlingstein P, **Cox P**, **Betts R**, **Bopp L**, **von Bloh W**, **Brovkin V**, **Cadule P**, **Doney S**, **Eby M**, **Fung I**, **Bala G**, **John J**, **Jones C**, **Joos F**, **Kato T**, **Kawamiya M**, **Knorr W**, **Lindsay K**, **Matthews HD**, **Raddatz T**, **Rayner P**, **Reick C**, **Roeckner E**, **Schnitzler K-G**, **Schnur R**, **Strassmann K**, **Weaver AJ**, **Yoshikawa C and Zeng N** (2006) Climate–carbon cycle feedback analysis: Results from the C4MIP model intercomparison. *Journal of Climate 19*(14), 3337–3353.

Friedlingstein P, **O'Sullivan M**, **Jones MW**, **Andrew RM**, **Hauck J**, **Landschützer P**, **Le Quéré C**, **Li H**, **Luijkx IT**, **Olsen A**, **Peters GP**, **Peters W**, **Pongratz J**, **Schwingshackl C**, **Sitch S**, **Canadell JG**, **Ciais P**, **Jackson RB**, **Alin SR**, **Arneth A**, **Arora V**, **Bates NR**, **Becker M**, **Bellouin N**, **Berghoff CF**, **Bittig HC**, **Bopp L**, **Cadule P**, **Campbell K**, **Chamberlain MA**, **Chandra N**, **Chevallier F**, **Chini LP**, **Colligan T**, **Decayeux J**, **Djeutchouang LM**, **Dou X**, **Duran Rojas C**, **Enyo K**, **Evans W**, **Fay AR**, **Feely RA**, **Ford DJ**, **Foster A**, **Gasser T**, **Gehlen M**, **Gkritzalis T**, **Grassi G**, **Gregor L**, **Gruber N**, **Gürses Ö**, **Harris I**, **Hefner M**, **Heinke J**, **Hurtt GC**, **Iida Y**, **Ilyina T**, **Jacobson AR**, **Jain AK**, **Jarníková T**, **Jersild A**, **Jiang F**, **Jin Z**, **Kato E**, **Keeling RF**, **Klein Goldewijk K**, **Knauer J**, **Korsbakken JI**, **Lan X**, **Lauvset SK**, **Lefèvre N**, **Liu Z**, **Liu J**, **Ma L**, **Maksyutov S**, **Marland G**, **Mayot N**, **McGuire PC**, **Metzl N**, **Monacci NM**, **Morgan EJ**, **Nakaoka S-I**, **Neill C**, **Niwa Y**, **Nützel T**, **Olivier L**, **Ono T**, **Palmer PI**, **Pierrot D**, **Qin Z**, **Resplandy L**, **Roobaert A**, **Rosan TM**, **Rödenbeck C**, **Schwinger J**, **Smallman TL**, **Smith SM**, **Sospedra-Alfonso R**, **Steinhoff T**, **Sun Q**, **Sutton AJ**, **Séférian R**, **Takao S**, **Tatebe H**, **Tian H**, **Tilbrook B**, **Torres O**, **Tourigny E**, **Tsujino H**, **Tubiello F**, **van der Werf G**, **Wanninkhof R**, **Wang X**, **Yang D**, **Yang X**, **Yu Z**, **Yuan W**, **Yue X**, **Zaehle S**, **Zeng N and Zeng J** (2025) Global carbon budget 2024. *Earth System Science Data 17*(3), 965–1039.

German DP, **Marcelo KRB**, **Stone MM and Allison SD** (2012) The Michaelis–Menten kinetics of soil extracellular enzymes in response to temperature: A cross-latitudinal study. *Global Change Biology 18*(4), 1468–1479.

Grigal DF and McColl JG (1975) Litter fall after wildfire in virgin forests of northeastern Minnesota. *Canadian Journal of Forest Research 5*(4), 655–661.

Hamdi S, **Moyano F**, **Sall S**, **Bernoux M and Chevallier T** (2013) Synthesis analysis of the temperature sensitivity of soil respiration from laboratory studies in relation to incubation methods and soil conditions. *Soil Biology and Biochemistry 58*, 115–126.

Hanson P, **Edwards N**, **Garten C and Andrews J** (2000) Separating root and soil microbial contributions to soil respiration: A review of methods and observations. *Biogeochemistry 48*(1), 115–146.

https://doi.org/10.1017/eds.2026.10034 Published online by Cambridge University Press

Holden SR, **Rogers BM**, **Treseder KK and Randerson JT** (2016) Fire severity influences the response of soil microbes to a boreal forest fire. *Environmental Research Letters 11*(3), 035004.

Jian J, **Bailey V**, **Dorheim K**, **Konings AG**, **Hao D**, **Shiklomanov AN**, **Snyder A**, **Steele M**, **Teramoto M**, **Vargas R and Bond-Lamberty B** (2022a) Historically inconsistent productivity and respiration fluxes in the global terrestrial carbon cycle. *Nature Communications 13*(1), 1733.

Jian J, **Frissell M**, **Hao D**, **Tang X**, **Berryman E and Bond-Lamberty B** (2022b) The global contribution of roots to total soil respiration. *Global Ecology and Biogeography 31*(4), 685–699.

Jian S, **Li J**, **Wang G**, **Kluber LA**, **Schadt CW**, **Liang J and Mayes MA** (2020) Multi-year incubation experiments boost confidence in model projections of long-term soil carbon dynamics. *Nature Communications 11*(1), 5864.

Kalyn AL and Van Rees KCJ (2006) Contribution of fine roots to ecosystem biomass and net primary production in black spruce, aspen, and jack pine forests in Saskatchewan. *Agricultural and Forest Meteorology 140*(1), 236–243.

Kelly J, **Ibáñez TS**, **Santín C**, **Doerr SH**, **Nilsson M-C**, **Holst T**, **Lindroth A and Kljun N** (2021) Boreal forest soil carbon fluxes one year after a wildfire: Effects of burn severity and management. *Global Change Biology 27*(17), 4181–4195.

Keuper F, **Wild B**, **Kummu M**, **Beer C**, **Blume-Werry G**, **Fontaine S**, **Gavazov K**, **Gentsch N**, **Guggenberger G**, **Hugelius G**, **Jalava M**, **Koven C**, **Krab EJ**, **Kuhry P**, **Monteux S**, **Richter A**, **Shahzad T**, **Weedon JT and Dorrepaal E** (2020) Carbon loss from northern circumpolar permafrost soils amplified by rhizosphere priming. *Nature Geoscience 13*(8), 560–565.

Köster K, **Aaltonen H**, **Köster E**, **Berninger F and Pumpanen J** (2024) Post-fire soil carbon emission rates along boreal forest fire chronosequences in Northwest Canada show significantly higher emission potentials from permafrost soils compared to non-permafrost soils. *Frontiers in Ecology and Evolution 11*, 1331018.

Köster K, **Berninger F**, **Lindén A**, **Köster E and Pumpanen J** (2014) Recovery in fungal biomass is related to decrease in soil organic matter turnover time in a boreal fire chronosequence. *Geoderma 235–236*, 74–82.

Köster E, **Köster K**, **Berninger F**, **Aaltonen H**, **Zhou X and Pumpanen J** (2017) Carbon dioxide, methane and nitrous oxide fluxes from a fire chronosequence in subarctic boreal forests of Canada. *Science of the Total Environment 601–602*, 895–905.

Kurganova I, **Teepe R and Loftfield N** (2007) Influence of freeze-thaw events on carbon dioxide emission from soils at different moisture and land use. *Carbon Balance and Management 2*(1), 2.

Luo Z, **Wang G and Wang E** (2019) Global subsoil organic carbon turnover times dominantly controlled by soil properties rather than climate. *Nature Communications 10*(1), 3688.

Luo Y, **Weng E**, **Wu X**, **Gao C**, **Zhou X and Zhang L** (2009) Parameter identifiability, constraint, and equifinality in data assimilation with ecosystem models. *Ecological Applications 19*(3), 571–574.

Maier M and Schack-Kirchner H (2014) Using the gradient method to determine soil gas flux: A review. *Agricultural and Forest Meteorology 192–193*, 78–95.

Männistö M, **Vuosku J**, **Stark S**, **Saravesi K**, **Suokas M**, **Markkola A**, **Martz F and Rautio P** (2018) Bacterial and fungal communities in boreal forest soil are insensitive to changes in snow cover conditions. *FEMS Microbiology Ecology 94*(9), fiy123.

Marschmann GL, **Pagel H**, **Kügler P and Streck T** (2019) Equifinality, sloppiness, and emergent structures of mechanistic soil biogeochemical models. *Environmental Modelling & Software 122*, 104518.

McLauchlan KK and Hobbie SE (2004) Comparison of labile soil organic matter fractionation techniques. *Soil Science Society of America Journal 68*(5), 1616–1625.

Metropolis N, **Rosenbluth AW**, **Rosenbluth MN**, **Teller AH and Teller E** (1953) Equations of state calculations by fast computing machines. *Journal of Chemical Physics 21*(6), 1087–1092.

Michaelis L and Menten M (1913) Die kinetik der invertin wirkung. *Biochemische Zeitschrift 49*, 334–336.

Mikan CJ, **Schimel JP and Doyle AP** (2002) Temperature controls of microbial respiration in arctic tundra soils above and below freezing. *Soil Biology and Biochemistry 34*(11), 1785–1795.

Moyano FE, **Manzoni S and Chenu C** (2013) Responses of soil heterotrophic respiration to moisture availability: An exploration of processes and models. *Soil Biology and Biochemistry 59*, 72–85.

Natural Resources Canada (2021) Canadian Wildland Fire Information System. Available at https://cwfis.cfs.nrcan.gc.ca/home (accessed March 29, 2021).

Neumann M, **Godbold DL**, **Hirano Y and Finér L** (2020) Improving models of fine root carbon stocks and fluxes in European forests. *Journal of Ecology 108*(2), 496–514.

Obu J, **Westermann S**, **Bartsch A**, **Berdnikov N**, **Christiansen HH**, **Dashtseren A**, **Delaloye R**, **Elberling B**, **Etzelmüller B**, **Kholodov A**, **Khomutov A**, **Kääb A**, **Leibman MO**, **Lewkowicz AG**, **Panda SK**, **Romanovsky V**, **Way RG**, **Westergaard-Nielsen A**, **Wu T**, **Yamkhin J and Zou D** (2019) Northern hemisphere permafrost map based on TTOP modelling for 2000–2016 at 1 km2 scale. *Earth-Science Reviews 193*, 299–316.

Paré D, **Laganière J**, **Larocque GR and Boutin R** (2022) Effects of a warmer climate and forest composition on soil carbon cycling, soil organic matter stability and stocks in a humid boreal region. *The Soil 8*(2), 673–686.

Perveen N, **Barot S**, **Alvarez G**, **Klumpp K**, **Martin R**, **Rapaport A**, **Herfurth D**, **Louault F and Fontaine S** (2014) Priming effect and microbial diversity in ecosystem functioning and response to global change: A modeling approach using the SYMPHONY model. *Global Change Biology 20*(4), 1174–1190.

Pierson D, **Lohse KA**, **Wieder WR**, **Patton NR**, **Facer J**, **de Graaff M-A**, **Georgiou K**, **Seyfried MS**, **Flerchinger G and Will R** (2022) Optimizing process-based models to predict current and future soil organic carbon stocks at high-resolution. *Scientific Reports 12*(1), 10824.

https://doi.org/10.1017/eds.2026.10034 Published online by Cambridge University Press

Reichstein M and Beer C (2008) Soil respiration across scales: The importance of a model–data integration framework for data interpretation. *Journal of Plant Nutrition and Soil Science 171*(3), 344–354.

Reynolds BC and Hunter MD (2001) Responses of soil respiration, soil nutrients, and litter decomposition to inputs from canopy herbivores. *Soil Biology and Biochemistry 33*(12), 1641–1652.

Ribeiro-Kumara C, **Köster E**, **Aaltonen H and Köster K** (2020) How do forest fires affect soil greenhouse gas emissions in upland boreal forests? A review. *Environmental Research 184*, 109328.

Richardson AD, **Williams M**, **Hollinger DY**, **Moore DJP**, **Dail DB**, **Davidson EA**, **Scott NA**, **Evans RS**, **Hughes H**, **Lee JT**, **Rodrigues C and Savage K** (2010) Estimating parameters of a forest ecosystem C model with measurements of stocks and fluxes as joint constraints. *Oecologia 164*(1), 25–40.

Richey M (2010) The evolution of Markov chain Monte Carlo methods. *The American Mathematical Monthly 117*(5), 383–413.

Ruess RW, **Hendrick RL**, **Burton AJ**, **Pregitzer KS**, **Sveinbjornssön B**, **Allen MF and Maurer GE** (2003) Coupling fine root dynamics with ecosystem carbon cycling in Black spruce forests of interior Alaska. *Ecological Monographs 73*(4), 643–662.

Running S, **Mu Q and Zhao M** (2022a) MOD17A2H MODIS/Terra Gross Primary Productivity 8-Day L4 Global 500m SIN Grid V006 [Data set]. Available at https://doi.org/10.5067/MODIS/MOD17A2H.006 (accessed May 24, 2022).

Running S, **Mu Q and Zhao M** (2022b) MYD17A2H MODIS/Terra Gross Primary Productivity 8-Day L4 Global 500m SIN Grid V006 [Data set]. Available at https://doi.org/10.5067/MODIS/MYD17A2H.006 (accessed May 24, 2022).

Running S and Zhao M (2019) Daily GPP and Annual NPP (MOD17A2H/A3H) and Year-end Gap- Filled (MOD17A2HGF/A3HGF) Products NASA Earth Observing System MODIS Land Algorithm (For Collection 6) (accessed December 20, 2022).

Ryan EM, **Ogle K**, **Kropp H**, **Samuels-Crow KE**, **Carrillo Y and Pendall E** (2018) Modeling soil CO2 production and transport with dynamic source and diffusion terms: Testing the steady-state assumption using DETECT v1.0. *Geoscientific Model Development 11*(5), 1909–1928.

Sacks WJ, **Schimel DS**, **Monson RK and Braswell BH** (2006) Model-data synthesis of diurnal and seasonal CO 2 fluxes at Niwot Ridge, Colorado. *Global Change Biology 12*(2), 240–259.

Sandholt I, **Rasmussen K and Andersen J** (2002) A simple interpretation of the surface temperature/vegetation index space for assessment of surface moisture status. *Remote Sensing of Environment 79*(2–3), 213–224.

Schaefer K and Jafarov E (2016) A parameterization of respiration in frozen soils based on substrate availability. *Biogeosciences 13*(7), 1991–2001.

Schuur EAG, **Bockheim J**, **Canadell JG**, **Euskirchen E**, **Field CB**, **Goryachkin SV**, **Hagemann S**, **Kuhry P**, **Lafleur PM**, **Lee H**, **Mazhitova G**, **Nelson FE**, **Rinke A**, **Romanovsky VE**, **Shiklomanov N**, **Tarnocai C**, **Venevsky S**, **Vogel JG and Zimov SA** (2008) Vulnerability of permafrost carbon to climate change: Implications for the global carbon cycle. *Bioscience 58*(8), 701–714.

Schwalm CR, **Williams CA**, **Schaefer K**, **Anderson R**, **Arain MA**, **Baker I**, **Barr A**, **Black TA**, **Chen G**, **Chen JM**, **Ciais P**, **Davis KJ**, **Desai A**, **Dietze M**, **Dragoni D**, **Fischer ML**, **Flanagan LB**, **Grant R**, **Gu L**, **Hollinger D**, **Izaurralde RC**, **Kucharik C**, **Lafleur P**, **Law BE**, **Li L**, **Li Z**, **Liu S**, **Lokupitiya E**, **Luo Y**, **Ma S**, **Margolis H**, **Matamala R**, **McCaughey H**, **Monson RK**, **Oechel WC**, **Peng C**, **Poulter B**, **Price DT**, **Riciutto DM**, **Riley W**, **Sahoo AK**, **Sprintsin M**, **Sun J**, **Tian H**, **Tonitto C**, **Verbeeck H and Verma SB** (2010) A model-data intercomparison of CO_2 exchange across North America: Results from the North American carbon program site synthesis. *Journal of Geophysical Research: Biogeosciences 115*(G3), G00H05.

Shao P, **Zeng X**, **Moore DJP and Zeng X** (2013) Soil microbial respiration from observations and earth system models. *Environmental Research Letters 8*(3), 034034.

Shi Z, **Crowell S**, **Luo Y and Moore B** (2018) Model structures amplify uncertainty in predicted soil carbon responses to climate change. *Nature Communications 9*(1), 2171.

Sihi D, **Gerber S**, **Inglett PW and Inglett KS** (2016) Comparing models of microbial– Substrate interactions and their response to warming. *Biogeosciences 13*(6), 1733–1752.

Sloan VL, **Fletcher BJ**, **Press MC**, **Williams M and Phoenix GK** (2013) Leaf and fine root carbon stocks and turnover are coupled across Arctic ecosystems. *Global Change Biology 19*(12), 3668–3676.

Song J, **Liu Z**, **Zhang Y**, **Yan T**, **Shen Z and Piao S** (2019) Effects of wildfire on soil respiration and its heterotrophic and autotrophic components in a montane coniferous forest. *Journal of Plant Ecology 12*(2), 336–345.

Subke J-A, **Hahn V**, **Battipaglia G**, **Linder S**, **Buchmann N and Cotrufo MF** (2004) Feedback interactions between needle litter decomposition and rhizosphere activity. *Oecologia 139*(4), 551–559.

Subke J-A, **Inglima I and Cotrufo MF** (2006) Trends and methodological impacts in soil CO2 efflux partitioning: A metaanalytical review. *Global Change Biology 12*(6), 921–943.

Sulman BN, **Moore J A M**, **Abramoff R**, **Averill C**, **Kivlin S**, **Georgiou K**, **Sridhar B**, **Hartman MD**, **Wang G**, **Wieder WR**, **Bradford MA**, **Luo Y**, **Mayes MA**, **Morrison E**, **Riley WJ**, **Salazar A**, **Schimel JP**, **Tang J and Classen AT** (2018) Multiple models and experiments underscore large uncertainty in soil carbon dynamics. *Biogeochemistry 141*(2), 109–123.

Tang J and Zhuang Q (2008) Equifinality in parameterization of process-based biogeochemistry models: A significant uncertainty source to the estimation of regional carbon dynamics. *Journal of Geophysical Research 113*, 13.

Taş N, **Prestat E**, **McFarland JW**, **Wickland KP**, **Knight R**, **Berhe AA**, **Jorgenson T**, **Waldrop MP and Jansson JK** (2014) Impact of fire on active layer and permafrost microbial communities and metagenomes in an upland Alaskan boreal forest. *The ISME Journal 8*(9), 1904–1919.

Tikhonov A-IN (1977) *Solutions of Ill Posed Problems*. Washington, NY: Wiley.

https://doi.org/10.1017/eds.2026.10034 Published online by Cambridge University Press

Todd-Brown KEO, **Hopkins FM**, **Kivlin SN**, **Talbot JM and Allison SD** (2012) A framework for representing microbial decomposition in coupled climate models. *Biogeochemistry 109*(1–3), 19–33.

Trudinger CM, **Raupach MR**, **Rayner PJ**, **Kattge J**, **Liu Q**, **Pak B**, **Reichstein M**, **Renzullo L**, **Richardson AD**, **Roxburgh SH**, **Styles J**, **Wang YP**, **Briggs P**, **Barrett D and Nikolova S** (2007) OptIC project: An intercomparison of optimization techniques for parameter estimation in terrestrial biogeochemical models. *Journal of Geophysical Research 112*(G2), G02027.

van Wijk MT, **van Putten B**, **Hollinger DY and Richardson AD** (2008) Comparison of different objective functions for parameterization of simple respiration models. *Journal of Geophysical Research 113*, G03008.

Vermote E and Wolfe R (2022a) MOD09GA MODIS/Terra Surface Reflectance Daily L2G Global 1kmand 500m SIN Grid V006 [Data set]. Available at https://doi.org/10.5067/MODIS/MOD09GA.006 (accessed June 9, 2022).

Vermote E and Wolfe R (2022b) MYD09GA MODIS/Aqua Surface Reflectance Daily L2G Global 1km and 500m SIN Grid V006 [Data set]. Available at https://doi.org/10.5067/MODIS/MYD09GA.006 (accessed June 9, 2022).

Walker XJ, **Baltzer JL**, **Cumming SG**, **Day NJ**, **Ebert C**, **Goetz S**, **Johnstone JF**, **Potter S**, **Rogers BM**, **Schuur EAG**, **Turetsky MR and Mack MC** (2019) Increasing wildfires threaten historic carbon sink of boreal forest soils. *Nature 572*(7770), 520–523.

Wan Z (1999) MODIS Land-Surface Temperature Algorithm Theoretical Basis Document (LST ATBD) (accessed December 20, 2022).

Wan Z (2013) MODIS Land Surface Temperature Products (accessed December 20, 2022).

Wan Z, **Hook S and Hulley G** (2015a) MOD11A2 MODIS/Terra Land Surface Temperature/Emissivity 8-Day L3 Global 1km SIN Grid V006 [Data set]. Available at https://doi.org/10.5067/MODIS/MOD11A2.006 (accessed May 28, 2022).

Wan Z, **Hook S and Hulley G** (2015b) MYD11A2 MODIS/Aqua Land Surface Temperature/Emissivity 8-Day L3 Global 1km SIN Grid V006 [Data set]. Available at https://doi.org/10.5067/MODIS/MYD11A2.006 (accessed May 28, 2022).

Wang X, **Chen G**, **Wang S**, **Zhang L and Zhang R** (2019) Temperature sensitivity of different soil carbon pools under biochar addition. *Environmental Science and Pollution Research 26*(4), 4130–4140.

Wang Y, **Liu H**, **Chung H**, **Yu L**, **Mi Z**, **Geng Y**, **Jing X**, **Wang S**, **Zeng H**, **Cao G**, **Zhao X and He J-S** (2014) Non-growing-season soil respiration is controlled by freezing and thawing processes in the summer monsoon-dominated Tibetan alpine grassland. *Global Biogeochemical Cycles 28*(10), 1081–1095.

Warner DL, **Bond-Lamberty B**, **Jian J**, **Stell E and Vargas R** (2019) Spatial predictions and associated uncertainty of annual soil respiration at the global scale. *Global Biogeochemical Cycles 33*(12), 1733–1745.

Wei H and Man X (2021) Increased litter greatly enhancing soil respiration in Betula platyphylla forests of permafrost region, Northeast China. *Forests 12*(1), 89.

Wiltshire S, **Grobe S and Beckage B** (2023) A historically driven Spinup procedure for soil carbon Modeling. *Soil Systems 7*(2), 35.

Woolf D and Lehmann J (2019) Microbial models with minimal mineral protection can explain long-term soil organic carbon persistence. *Scientific Reports 9*(1), 6522.

Wutzler T and Reichstein M (2013) Priming and substrate quality interactions in soil organic matter models. *Biogeosciences 10*(3), 2089–2103.

Xia JY, **Luo YQ**, **Wang Y-P**, **Weng ES and Hararuk O** (2012) A semi-analytical solution to accelerate spin-up of a coupled carbon and nitrogen land model to steady state. *Geoscientific Model Development 5*(5), 1259–1271.

Zhang Y, **Xu M**, **Chen H and Adams J** (2009) Global pattern of NPP to GPP ratio derived from MODIS data: Effects of ecosystem type, geographical location and climate. *Global Ecology and Biogeography 18*(3), 280–290.

Zhang F, **Zhang L-W**, **Shi J-J and Huang J-F** (2014) Soil moisture monitoring based on land surface temperature-vegetation index space derived from MODIS data. *Pedosphere 24*(4), 450–460.

Zhao B, **Zhuang Q**, **Shurpali N**, **Köster K**, **Berninger F and Pumpanen J** (2021) North American boreal forests are a large carbon source due to wildfires from 1986 to 2016. *Scientific Reports 11*(1), 7723.

Zobitz J, **Aaltonen H**, **Zhou X**, **Berninger F**, **Pumpanen J and Köster K** (2021) Comparing an exponential respiration model to alternative models for soil respiration components in a Canadian wildfire chronosequence (FireResp v1.0). *Geoscientific Model Development 14*(10), 6605–6622.

Zobitz J, **Desai A**, **Moore D and Chadwick M** (2011) A primer for data assimilation with ecological models using Markov chain Monte Carlo (MCMC). *Oecologia 167*(3), 599–611.

Zobitz J, **Moore DJP**, **Sacks WJ**, **Monson RK**, **Bowling DR and Schimel DS** (2008) Integration of process-based soil respiration models with whole-ecosystem CO2 measurements. *Ecosystems 11*(2), 250–269.

Zobitz J, **Quaife T and Nichols N** (2019) Efficient hyper-parameter determination for regularised linear BRDF parameter retrieval. *International Journal of Remote Sensing 41*, 1–21.

Zomorrodi AR and Segrè D (2016) Synthetic ecology of microbes: Mathematical models and applications. *Journal of Molecular Biology 428*(5, Part B), 837–861.

Cite this article: Zobitz J, Zhou X, Aaltonen H, Köster E, Berninger F, Pumpanen J and Köster K (2026). Combined effects of site and model parameterization for soil respiration components in a Canadian wildfire chronosequence. *Environmental Data Science*, 5: e7. doi:10.1017/eds.2026.10034

https://doi.org/10.1017/eds.2026.10034 Published online by Cambridge University Press